A WIND TUNNEL STUDY OF THE LIFT-DRAG RATIO ON A CAMBERED CIRCULATION CONTROLLED ELLIPTICAL AIRFOIL

Thomas A. Stevenson

Air Force Institute of Technology
Wright-Patterson Air Force Base, Ohio

June 1974

SECURITY CLASSIFICATION OF THIS PAGE (When Data Entered)

REPORT DOCUMENTATION PAGE		READ INSTRUCTIONS BEFORE COMPLETING FORM
1. REPORT NUMBER GAM/AE/74-1	2. GOVT ACCESSION NO.	3. RECIPIENT'S CATALOG NUMBER AD A023361
4. TITLE (and Subtitle) A WIND TUNNEL STUDY OF THE LIFT-DRAG RATIO ON A CAMBERED CIRCULATION CONTROLLED ELLIPTICAL AIRFOIL		5. TYPE OF REPORT & PERIOD COVERED MS Thesis 6. PERFORMING ORG. REPORT NUMBER
7. AUTHOR(s) Thomas A. Stevenson Captain USAF		8. CONTRACT OR GRANT NUMBER(s)
9. PERFORMING ORGANIZATION NAME AND ADDRESS Air Force Institute of Technology (AFIT/EN) Wright-Patterson AFB, Ohio 45433		10. PROGRAM ELEMENT, PROJECT, TASK AREA & WORK UNIT NUMBERS
11. CONTROLLING OFFICE NAME AND ADDRESS Aeronautical Systems Division (ASD/XRHD) Wright-Patterson AFB, Ohio 45433		12. REPORT DATE June 1974 13. NUMBER OF PAGES 92
14. MONITORING AGENCY NAME & ADDRESS(if different from Controlling Office)		15. SECURITY CLASS. (of this report) Unclassified 15a. DECLASSIFICATION/DOWNGRADING SCHEDULE

16. DISTRIBUTION STATEMENT (of this Report)

Approved for public release; distribution unlimited.

17. DISTRIBUTION STATEMENT (of the abstract entered in Block 20, if different from Report)

[illegible] SUBJECT TO [illegible]

18. SUPPLEMENTARY NOTES

Approved for public release; IAW AFR 190-17

JERRY C. HIX, Captain, USAF
Director of Information

19. KEY WORDS (Continue on reverse side if necessary and identify by block number)

Airfoil Testing
Boundary Layer Control
Blowing
Circulation Control
High Lift Devices

20. ABSTRACT (Continue on reverse side if necessary and identify by block number)

See Reverse side.

DD FORM 1 JAN 73 1473 EDITION OF 1 NOV 65 IS OBSOLETE

Block #20

A wind tunnel study was conducted to determine the effect on the lift-to-drag ratio of adding a splitter plate to a 20 percent thick, five percent cambered, circulation controlled elliptical airfoil. The splitter plate was located on the lower surface of the airfoil at the 99 percent chord. The splitter plate was found to increase the lift-to-drag ratios of the circulation controlled airfoil. The splitter plate increased the section lift coefficient and decreased the section profile drag coefficient.

The maximum lift-to-drag ratio with the splitter plate was 56:1 which was accomplished at a momentum coefficient of 0.021 and -1 degree angle of attack. At a Reynolds number of 1.1×10^6 the splitter increased the lift-to-drag ratio of the airfoil between -6 and 3 degrees angle of attack. At a Reynolds number of 7.5×10^5 the splitter plate increased the lift-to-drag ratio of the airfoil between -6 and 6 degrees angle of attack.

A WIND TUNNEL STUDY OF THE LIFT-DRAG RATIO ON A CAMBERED CIRCULATION CONTROLLED ELLIPTICAL AIRFOIL

THESIS

GAM/AE/74-1 Thomas A. Stevenson
Captain USAF

A-b

A WIND TUNNEL STUDY OF THE LIFT-DRAG RATIO ON A CAMBERED CIRCULATION CONTROLLED ELLIPTICAL AIRFOIL

THESIS

Presented to the Faculty of the School of Engineering
of the Air Force Institute of Technology
Air University
in Partial Fulfillment of the
Requirements for the Degree of
Master of Science
by

Thomas A. Stevenson, B.S.
Captain USAF

Graduate Aerospace-Mechanical Engineering

June 1974

1 C

Preface

This thesis investigated the effect of a splitter plate on the lift-to-drag ratio of a cambered circulation controlled elliptical airfoil. The splitter plate which was located on the lower surface of the airfoil at the 99 percent chord, improved the lift and the lift-to-drag ratio of the airfoil. It is hoped that the results presented in this thesis will stimulate more research towards increasing the lift-to-drag ratio on circulation controlled devices.

I would like to express my appreciation to Dr. Milton E. Franke, my advisor, Professor Harold C. Larsen, and Mr. James Snyder, ASD/XRHD, for their assistance throughout the project. Special thanks go to Messrs. Millard Wolfe and Jack G. Tiffany, Jr. of the AFIT workshop. Their help in the design of the model and Mr. Tiffany's construction of an effective model airfoil contributed immeasurably to the success of the project. Thanks also go to Messrs. S. W. Whitt and T. Lokai for their advice and assistance with the apparatus in the wind tunnel.

In addition, sincere appreciation goes to Mr. Julius Becsey, Chemical Engineer, ARL, who wrote the computer programs for the data reduction and provided guidance in the reduction of the pressure data. Also thanks go to Mr. Henry Maurer, ASD Photography Laboratory, who provided assistance in photographing the pressure data. Finally, thanks go to my wife Robyn for her help and patience throughout the entire project.

Contents

List of Figures

Figure Page

List of Tables

List of Symbols

English Letters

b	Chord length of the splitter plate, in.
c	Chord length of the airfoil model, ft
C_p	Pressure coefficient
C_{p_ℓ}	Pressure coefficient on the lower surface of the airfoil
C_{p_u}	Pressure coefficient on the upper surface of the airfoil
c_d	Section profile drag coefficient
c_{d_t}	Section total drag coefficient
c_ℓ	Section lift coefficient
c_n	Section normal force coefficient
C_μ	Momentum coefficient
h	Wind tunnel test section height, ft
$\frac{\ell}{d}$	Section lift-to-total drag ratio
$\dot{m}$	Mass flow rate, lb_m/sec
P_j	Static pressure at the slot, psia
P_ℓ	Local static pressure, psfg
P_o	Free stream static pressure, psfg
P_t	Total pressure of the plenum chamber, psia
q	Local dynamic pressure, psfg
q_o	Free stream dynamic pressure, psfg
R	Universal gas constant, $\frac{ft^2}{sec^2\ R}$
Re	Reynolds number
S	Span of the airfoil model, ft
T_j	Temperature of the blowing air, R
V_j	Velocity at the slot, ft/sec
V_o	Free stream velocity, ft/sec

x Chordwise ordinate, ft

y Vertical ordinate, ft

Greek Letters

α_g Geometric angle of attack, degrees

β Splitter plate deflection from model chord line, degrees

γ Ratio of specific heats

Abstract

A wind tunnel study was conducted to determine the effect on the lift-to-drag ratio of adding a splitter plate to a 20 percent thick, five percent cambered, circulation controlled elliptical airfoil. The splitter plate was located on the lower surface of the airfoil at the 99 percent chord. The splitter plate was found to increase the lift-to-drag ratios of the circulation controlled airfoil. The splitter plate increased the section lift coefficient and decreased the section profile drag coefficient.

The maximum lift-to-drag ratio with the splitter plate was 56:1 which was accomplished at a momentum coefficient of 0.021 and -1 degree angle of attack. At a Reynolds number of 1.1×10^6 the splitter plate increased the lift-to-drag ratio of the airfoil between -6 and 3 degrees angle of attack. At a Reynolds number of 7.5×10^5 the splitter plate increased the lift-to-drag ratio of the airfoil between -6 and 6 degrees angle of attack.

I. Introduction

During the past decade there has been a renewed interest in devices that improve the low-speed, high-lift capabilities of an aircraft. The primary motivation for the renewed interest has been the requirement that all types of aircraft must be able to takeoff and land in shorter distances. Not only must a STOL transport have short takeoff and landing characteristics, but a high-speed fighter must also be able to demonstrate a low-speed, high-lift capability during takeoff and landing. In addition, the low-speed, high-lift device has use in cruise flight. For example, reconnaissance and forward control aircraft may be required to loiter over targets at low speeds. A high-lift device with low drag characteristics would help an aircraft accomplish this mission.

One low-speed, high-lift device that has undergone considerable study is circulation control. Circulation control on an airfoil is the use of a jet of air to re-energize the airfoil surface boundary layer. When a jet nozzle is placed near the trailing edge of a blunt end airfoil a sufficiently strong jet of air can transfer the separation point to the lower surface of the airfoil. As a result, both the forward and rear stagnation points move to the lower surface and cause the airfoil to have a high lift coefficient and a low pressure drag coefficient.

Previous Work

Previous experimental studies of circulation control on airfoils have emphasized the additional lift that can be obtained through its use. Kind (Ref 5) obtained section lift coefficients as high as 3.2. Williams (Ref 14) and Walters (Ref 13) obtained section lift coefficients of 6.3 and 4.58 respectively. These coefficients were obtained on airfoils with a modified circular trailing edge.

Kind found that circulation control has several advantages as a high-lift device. The important advantages are mechanical simplicity and the ability to generate a large lift force at small and even negative angles of attack while using small amounts of blowing. However, he also found that the lift-to-drag ratio was only 30:1. The relatively high drag was attributed to mixing losses associated with the separation of the blowing air from the trailing edge of the airfoil and the power required to blow the air through the slot.

Kind found that by using a small flat plate, or splitter plate, attached to the lower surface near the trailing edge of the airfoil, the mixing losses could be reduced and the lift-to-drag ratio improved. However, Kind's work was preliminary and more experimental effort is required to determine the effect of a splitter plate on the lift-to-drag ratio of circulation controlled devices.

Present Study

The purpose of this study was to conduct wind tunnel tests on a circulation controlled airfoil with and without a splitter plate and to determine the improvement in the lift-to-drag ratio. Also, the effect of the splitter plate chord length on the lift-to-drag ratio was investigated. The study was limited to two aspects of the total drag problem. These were to reduce the mixing losses associated with the separation of the jet of air from the surface of the airfoil, and to lower the amount of blowing required to obtain high section lift coefficients.

The study was conducted on an elliptical airfoil. The elliptical airfoil was used in this study for three reasons. First, the elliptical airfoil has the blunt trailing edge required to produce the circulation control. Second, there have been previous studies conducted using elliptical airfoils which were available for comparison. Finally, the potential flow pressure distribution on the airfoil can be computed. In this study the potential flow pressure distribution was determined with a computer program that used the Theodorsen transformation. Figure 1 shows a cross section of an elliptical airfoil.

Scope

This study was conducted in two phases. During the first phase the airfoil characteristics that affect the lift and drag were investigated through the use of potential

flow theory and the experience gained by others from previous tests and studies. These characteristics were the shape of the airfoil, the shape of the trailing edge, and the locations of the slot and splitter plate on the airfoil. Finally, a model airfoil was designed to increase the lift-to-drag ratio of Kind's model by adding camber and a pure ellipse trailing edge to the airfoil design used by Kind.

The second phase of the study was to test a model of the airfoil in the AFIT Five-Foot Wind Tunnel. The tests were conducted at two Reynolds numbers, 1.1×10^6 and 7.6×10^5, at a range of momentum coefficients from 0.01 to 0.046. The higher momentum coefficients were obtained at the lower Reynolds number. Tests were conducted with and without the splitter plate at a range of geometric angles of attack from -6 to 16 degrees. Also, the chord length of the splitter plate was varied during the tests.

II. Preliminary Investigation

The purpose of the preliminary investigation was to design a circulation controlled airfoil for lift-to-drag ratios better than 30:1. Four parameters were examined. They were the airfoil shape, the trailing edge shape, the slot location, and the splitter plate location.

The effect of the airfoil shape on both the lift and drag characteristics of the elliptical airfoil was studied through potential flow theory. Theodorsen's transformation was used to examine the pressure distribution on several different airfoils. It was found that the addition of five percent camber to a 20 percent thick elliptical airfoil would significantly reduce the adverse pressure gradient at both the leading and trailing edges of the airfoil while producing an equal lift force. Figure 2 shows the pressure distribution on a 20 percent elliptical airfoil with and without camber.

The effect of the geometric shape of the trailing edge on the lift and drag was studied through the experience of Englar (Ref 3), Kind, Walters, and Williams. All four used a circular trailing edge on an elliptical airfoil to attain increased lift coefficients with circulation control. The circular trailing edge of the airfoils provided a large radius of curvature that was conducive to effective turning of the jet of air as it left the slot. However, this same strong attachment resulted in flow separation on the lower

surface of the airfoil. Thus, strong mixing losses were evident with the rounded trailing edge. Englar found that while a pure ellipse trailing edge did not produce as large a lift force as the circular trailing edge, it did produce a better lift-to-drag ratio at the same momentum coefficient. The lower lift on the pure ellipse was a result of the smaller radius of curvature and the less effective turning of the blowing air. However, the mixing losses were reduced since separation took place very near the trailing edge of the airfoil.

Since the purpose of the splitter plate is to reduce mixing losses on the lower surface of the airfoil, it must be located close to the trailing edge on the lower surface. However, the plate must allow sufficient surface area on the trailing edge of the airfoil for good blowing air attachment. The location of the splitter plate dictates the location of the separation of the flow from the surface. Therefore, the splitter plate was located at the 99 percent chord on the lower surface. Figure 3 shows a comparison of the flow on a circular trailing edge with the flow on an elliptical trailing edge which has a splitter plate.

The slot location was also found to be an important factor in improving lift-to-drag ratios. When the slot is moved forward a larger momentum coefficient is required to produce effective turning of the blowing air at a fixed angle of attack. If the slot is moved too far aft the momentum coefficient must increase as the angle of attack

increases. The increase in momentum coefficient is necessary in order to prevent separation of the re-energized flow. Potential flow theory also revealed that the slot should be placed just forward of the adverse pressure gradient at the trailing edge of the airfoil.

As a result of the preliminary investigation, a model elliptical airfoil designed for lift-to-drag ratios larger than 30:1 was constructed for tests in the AFIT Five-Foot Wind Tunnel. The model airfoil was different from Kind's model in that it had five percent camber and a pure ellipse trailing edge. Figure 4 shows a comparison of the cross sections of the two models.

III. Description of Apparatus

Wind Tunnel

Wind tunnel tests were performed in the Air Force Institute of Technology Five-Foot Wind Tunnel. The tunnel is an open circuit type wind tunnel with a maximum flow speed of 300 miles per hour. Two large plyboard side panels were installed in the five-foot diameter circular test section. These panels created a two-dimensional test section which was 60 inches high and 30 inches wide. The trailing edges of the panels were hinged and attached to servos. Four pitot-static tubes were installed on the top, bottom, right side and left side of the entrance to the two-dimensional test section. These pitot-static tubes measured the local dynamic pressure q. The trailing edges of the two side panels were adjusted during the tests to insure that the local q's were equal. As a result, a more uniform flow existed in the test section. Figure 5 shows the test section.

The tunnel head was measured by comparing the static pressure at the entrance to the test section with atmospheric pressure. The static pressure at the entrance to the test section was measured by eight static ports evenly spaced around the circumference of the tunnel. The difference between atmospheric pressure and the tunnel static pressure was recorded on a micro-manometer filled with water and designated the tunnel head or "tunnel q."

The turbulence factor of the tunnel was 1.5. This factor accounted for the turbulence in the wind tunnel caused by the propeller, the guide vanes and the vibration of the tunnel walls. However, the Reynolds numbers contained in this report do not contain this factor and they must be multiplied by 1.5 to obtain the effective Reynolds number. The effective Reynolds number should be used to compare the data in this report with data obtained in flight tests.

Airfoil

The model airfoil was a 20 percent thick elliptical airfoil with five percent camber. Since the shape of the trailing edge was not modified the airfoil was symmetrical about the front and rear. The chord of the airfoil was 1.67 feet and the span 2.17 feet. Figure 6 shows a sketch of the cross section of the airfoil model and Figure 7 shows a sketch of the top view of the model.

The airfoil was equipped with 48 surface static pressure taps. Tables I and II show the location of each of the taps. The 44 pressure taps located at the center span were used to measure the pressure distribution about the airfoil and the four pressure taps located off the center span were used to check the uniformity of the flow across the span of the model. Three pitot tubes were located in the plenum chamber to measure plenum total pressure and to check the spanwise uniformity of the flow going out of the slot.

The model had large circular aluminum endplates fitted to each side. The endplates were 0.1875 inches thick and beveled to 30 degrees at the edges. The purpose of the endplates was to strip off the boundary layer that formed on the plyboard side panels and aid in making the flow more two dimensional. However, when the model was mounted in the tunnel the endplates were 1.75 inches from the side panels. This distance was a compromise between placing the endplates far enough into the boundary layer and allowing enough space between the endplates and side panels to permit configuration changes on the model.

The left endplate also served as attachment points for the angle-of-attack drive mechanism. Two cables were attached to the fore and aft edges of the endplate, extended through the tunnel floor, and attached to a motor driven gear box. The motor, in turn, was connected to a revolution counter which was calibrated to an accuracy of three minutes of arc.

The blowing air system in the model consisted of an annealed copper pipe and a fiberglass plenum chamber. Both the chamber and the pipe extended across the span of the model. Figure 6 shows a sketch of the cross section of the pipe and plenum chamber. Blowing air entered the pipe through an opening in the left side of the model. From the pipe the air entered the plenum chamber which was constructed in the shape of a diverging-converging nozzle.

Figure 7 shows a sketch of the blowing air flow. Finally, the blowing air entered the slot which was the minimum area of the converging portion of the plenum chamber.

The slot was located on the upper surface of the airfoil at the 96 percent chord and extended across the span of the model. The 0.020 inch thick slot was fixed at a thickness to chord ratio of 0.0001 and was uniform to $\pm$ 0.0015 inches along the span of the model. Figure 8 shows a cross section of the slot and the trailing edge of the airfoil model.

Four configurations of the airfoil model were tested. The four configurations were designated Model A, Model B, Model C and Model D. Model A was the airfoil model without the splitter plate. Model B had a splitter plate attached on the lower surface of the model at the 99 percent airfoil chord. The chord of the splitter plate was 1.5 inches and was deflected 47 degrees from the airfoil chordline. Figure 8 shows a sketch of the trailing edge configurations of Model A and Model B. Model C was different from Model B in that the chord of the splitter plate was 1.0 inch and was deflected 46.5 degrees from the airfoil chordline. Finally, Model D had a splitter plate with a 0.5 inch chord which was deflected 47 degrees from the airfoil chordline. Figure 9 shows a sketch of the trailing edge configurations of Model C and Model D.

Flowmeter

The flowmeter used to measure the mass flow rate was a one inch inside diameter pipe which contained a 0.75 inch square edged orifice in the orifice plate. The temperature of the blowing air was measured by a mercury thermometer upstream of the orifice while a copper-constantan thermocouple was used downstream of the orifice. The flowmeter was calibrated against a Cox Instruments GL-12 Gas Turbine Flowmeter to an accuracy of $\pm$ 5 percent.

Wake Survey Rake

A total head wake survey rake was positioned 30 inches behind the airfoil. The rake had 115 total head tubes and six static pressure tubes. However, the manometer bank connected to the rake contained only 100 tubes so 94 total head tubes and six static pressure tubes were connected to the manometer bank. Figure 10 is a sketch of the wake survey rake.

Manometers

Two banks of manometers were used to measure the pressure on the airfoil surface and the rake. A 96 inch, 100-tube bank of vertical manometers which contained alcohol was connected to pressure taps on the airfoil. A 35 mm camera was positioned so that 46 tubes of the bank could be photographed during tests on the airfoil.

The rake was connected to a 30 inch, 100-tube bank of manometers which contained red oil. The bank was inclined 60 degrees from the vertical so that pressure changes on the rake could be read more accurately. A 70 mm camera was also inclined 60 degrees to the vertical and positioned so that photographs of the bank contained all 100 tubes.

Pitot Tube

A small pitot tube was constructed to measure the slot spanwise total pressure distribution. The outside diameter was 0.018 inches so that the pitot tube was able to fit into the slot.

IV. Experimental Procedure

Preliminary Tests

The model and wake survey rake were positioned in the tunnel as shown in Figure 5. However, before the actual wind tunnel tests were conducted several preliminary tests were performed on the model and associated apparatus. These tests included checks for air leaks from the tubing connecting the model and wake survey rake to the manometer banks, calibrating both the flowmeter and angle of attack counter, and aligning and testing camera equipment. Also, a tuft study and slot total pressure survey were conducted on the model.

General Procedure

The same general test procedure was used on each of the four model configurations. Each test started with the blowing air flowing from the slot and the mass flow rate held constant. The tunnel was then brought to tunnel speed. Next, the angle of attack was varied from -6 to 16 degrees. The test was started with the angle of attack at zero degrees. It was then changed to -6 degrees. From -6 to 16 degrees the angle of attack was changed in increments of two degrees except from -2 to 6 degrees when the increment was one degree. From 16 to zero degrees repeat data was taken in intervals of four degrees. Also, several complete tests were repeated on each model configuration. The results were compared to previous tests and checked for repeatability.

During each test the temperatures and pressures were recorded. Photographs were taken of the two manometer banks to simultaneously record the pressure data from the surface of the airfoil and wake survey rake.

V. Reduction of Data

The data obtained during the wind tunnel tests were reduced to three primary parameters. These parameters were the momentum coefficient, the section lift coefficient, and the section total drag coefficient. These three parameters were then used to calculate the lift-to-drag ratios of the different model configurations.

Momentum Coefficient

The momentum coefficient for this two-dimensional study is defined as

$$C_\mu = \frac{\dot{m} V_j}{q_o c} \tag{1}$$

where $\dot{m}$ is the mass flow rate per unit span, V_j the velocity of the jet of the slot, q_o the free stream dynamic pressure and c the chord length of the airfoil.

The velocity of the flow at the slot was found by assuming isentropic expansion from plenum chamber total pressure to slot static pressure according to the equation:

$$V_j = \left[2RT_j \left(\frac{\gamma}{\gamma-1}\right)\left[1 - \left(\frac{P_j}{P_t}\right)^{\frac{\gamma-1}{\gamma}}\right]\right]^{\frac{1}{2}} \tag{2}$$

The temperature in the plenum chamber was assumed to be equal to that of the flowmeter. The plenum chamber total pressure was measured on a mercury manometer and the static pressure of the slot was measured on the first static pressure tap immediately downstream of the slot.

Section Lift Coefficient

The section lift coefficient was determined by numerical integration of the pressure coefficients around the airfoil. The pressure coefficient is defined as:

$$C_p = \frac{P_\ell - P_o}{q_o} \tag{3}$$

The integration was performed using the trapezoidal rule of integration according to the equation

$$c_n = \int_0^1 (C_{p_\ell} - C_{p_u}) \quad d(\frac{x}{c}) \tag{4}$$

from Walters where c_n is the section normal force coefficient. The section lift coefficient was calculated from the equation:

$$c_\ell = c_n \cos\alpha_g \tag{5}$$

The integration of the pressure coefficients was performed on the Hewlett and Packard 9100A Calculator with 9107A Digitizer. The procedure is described in Appendix B. Several computations were performed by hand using the trapezoidal rule of integration and the largest difference between the two procedures was 2.3 percent.

Section Total Drag Coefficient

The total drag on a circulation controlled airfoil must include the drag associated with blowing air out of a slot. Kind defined the section total drag coefficient to be equal to

$$c_{d_t} = c_d + C_\mu \tag{6}$$

where c_d is the section profile drag coefficient determined from the wake survey rake and C_μ is the momentum coefficient.

The section profile drag coefficient was calculated by the momentum method from Pope (Ref 10). The momentum method compares the momentum ahead of the model with the momentum behind the airfoil. Thus the loss in momentum is defined as the profile drag of the airfoil. The profile drag was determined by an integration over the cross section of the tunnel using the wake survey rake and the equation

$$c_d = \frac{2}{c} \int_0^h \left[\sqrt{\frac{q}{q_o}} - \frac{q}{q_o} \right] dy \tag{7}$$

from Pope. The integration was performed by the trapezoidal rule of integration on the Hewlett and Packard 9100A Calculator with 9107A Digitizer. The procedure is described in Appendix C.

The momentum method assumes that all of the momentum originates ahead of the model. When blowing is applied this assumption is not valid because some momentum originates inside the model. As a result, the section profile drag coefficient obtained from the momentum method was corrected by the addition of the term

$$\frac{\dot{m} V_o}{q_o c} \tag{8}$$

from Englar.

Finally, the section total drag coefficient was determined by the equation:

$$c_{d_t} = c_d + C_\mu \tag{6}$$

Lift-to-Drag Ratio

The lift-to-drag ratio was computed by taking the ratio of the section lift coefficient to the section total drag coefficient. Therefore, the equation is:

$$\frac{l}{d} = \frac{c}{c_{d_t}} \tag{9}$$

Standard Correction Factors

Since the wind tunnel had solid boundaries, the results from wind tunnel tests were not the same as those that would have been obtained in the free atmosphere. The solid boundaries of the tunnel tended to restrain or block the flow. Correction factors for solid blocking, streamline curvature and wake blocking were applied to the data. Solid blocking accounted for the presence of the model in the wind tunnel test section which caused the free stream velocity to increase as it flowed over the model. The correction for solid blocking was a four percent decrease in the section profile drag coefficient and a three percent decrease in the section lift coefficient. Streamline curvature accounted for the presence of the ceiling and floor in the wind tunnel which prevented the normal curvature of the airflow. The airfoil appeared to have more camber than it actually had. As a result, the section lift coefficient was decreased by two percent. The wake blocking correction factor was less than one percent for both the section lift coefficient and section profile drag coefficient. Finally, a correction factor of 1.8 percent

was applied to the static pressure readings on the rake. This correction factor accounted for the errors in the static pressure readings due to the thickness of the rake.

The effectiveness of the correction factors was confirmed by the close agreement of the lift data with potential flow theory and the agreement of the lift and drag data obtained from previous studies. Figures 11 through 15 show the agreement between the potential flow pressure distributions and the experimental pressure distributions on various model configurations under various test conditions.

Downwash Correction Factors

During the wind tunnel tests the air flow was not truly two-dimensional. Three-dimensional effects were introduced by tip and wall vortices. The vortices caused the free stream velocity vector to be changed by an unknown downwash velocity. As a result, the two-dimensional geometric angles of attack were not the true effective angles of attack.

Ness (Ref 7) gives a method to find the true effective angle of attack provided the experimental pressure distribution is known. The method is to match the experimental pressure distribution with a potential flow pressure distribution at the same section lift coefficient but different angle of attack. The potential flow effective angle of attack is varied through trial and error until the pressure distributions are matched. The potential

flow effective angle of attack is the true effective angle of attack for the test condition.

Ness' procedure was accomplished on some data and the difference between the geometric angle of attack and effective angle of attack was as much as 0.5 degrees. However, Ness' procedure is tedious to apply and matches were not made on all the data taken in this study. As a result, only the geometric angle of attack is known precisely for each set of data.

VI. Results and Discussion

Preliminary Tests

A tuft study and slot total pressure survey were performed on the model before the actual wind tunnel tests. The tuft study indicated that the flow across the model and at the slot was essentially two-dimensional. However, there was evidence of vorticity at the junction of the model and endplates. Also, evidence of separation on the upper surface during blowing was detected. The separation usually occurred between angles of attack of two and four degrees.

The slot total pressure survey indicated that the flow from the slot was essentially uniform. The survey was taken by inserting a small pitot tube into the slot at various positions along the span of the model. Once the pitot tube was aligned with the flow, the total pressure was recorded. The results of the survey are presented in Table III. Also, Figure 16 shows the velocity at the slot for the various momentum coefficients presented in Table III. The velocity of the flow from the slot was uniform to $\pm$ 5 percent. The variations in velocity were probably due to slight irregularities in the thickness of the slot and moisture in the blowing air.

Test Observations

The data revealed two phenomena that occurred throughout the wind tunnel tests. First, the flow would separate from the trailing edge of the airfoil during blowing.

Separation occurred when the blowing air was not strong enough to re-energize the boundary layer so it would attach to the surface of the blunt trailing edge. The separation of the flow was caused by the location of the slot, the small radius of curvature of the pure ellipse, and the relatively small momentum coefficients used during the tests. At a Reynolds number of 1.1×10^6 and a momentum coefficient equal to 0.020 the separation occurred between angles of attack of two to five degrees on all model configurations. However, when the Reynolds number was decreased to 7.6×10^5 and the momentum coefficient increased to 0.042 the separation occurred between angles of attack of three to eight degrees.

While separation occurred at about the same angle of attack on models with and without the splitter plate, the section characteristics were different during separation. Figure 17 shows that the decrease of the section lift coefficient on the model without the splitter plate was abrupt, while the decrease on the model with the splitter plate was neither as great nor as abrupt. Also, the data obtained after separation was extremely scattered on the model with the splitter plate. Figure 18 shows that the rise in section total drag coefficient was only slight on both models immediately after separation. However, the drag began to rise rapidly at higher angles of attack. Also drag data became extremely scattered because of shear

layers and turbulence caused by the unattached blowing air. As a result of the scatter in the data after separation, only the section characteristics up to separation are presented.

The second phenomenum that was observed during the tests was a dip in the lift slopes of the model without the splitter plate. In Figure 19 there is a dip in the lift curve of the model without blowing. This dip was probably caused by the transition of the boundary layer from laminar flow to turbulent flow. The transition was observed on the manometer board during the tests. Also Patrick (Ref 9) observed the same phenomenum during wind tunnel tests in the same wind tunnel under similar test conditions. The transition of the flow occurred primarily because the surface of the model was not rough enough to ensure turbulent flow throughout the entire range of angles of attack for all model configurations.

The blowing air and splitter plate seemed to have an effect on the angle of attack at which transition occurred. When blowing air was applied to the model without the splitter plate the dip occurred at lower angles of attack. Figure 19 shows that the dip occurred at an angle of attack of zero degrees and momentum coefficient of 0.023. This occurred because the blowing air was essentially turbulent. At a Reynolds number of 1.1×10^6 the velocity at the slot was three to four times as great as the free stream velocity depending on the momentum coefficient. When the Reynolds number was decreased to 7.6×10^5 the velocity at the slot

was five times as great as the free stream velocity. The increased velocity at the slot caused the velocity of the laminar flow to increase and become turbulent at lower angles of attack.

The splitter plate also increased the velocity of the flow over the airfoil and caused the flow to become turbulent at low angles of attack. In fact, the splitter plate and blowing seemed to make the boundary layer turbulent throughout the range of angles of attack that were used in the tests. The fact that the boundary layer was turbulent was confirmed by the absence of dips in the lift curves of the models with the splitter plates and blowing.

Lift Results

The lift results are presented in Figures 19 through 24. Figure 19 shows that the blowing air increased the section lift coefficient on the model without the splitter plate. As the momentum coefficient increased so did the section lift coefficient. However, the splitter plates also increased the section lift coefficient. Figure 20 shows that as the splitter plate chord increased so did the section lift coefficient.

Figures 21 through 23 show that the blowing increased the section lift coefficient on each of the three models with the splitter plates. Also, Figure 24 shows that as the splitter plate chord increased so did the section lift coefficient at similar momentum coefficients. Thus both the splitter plate and the blowing increased the section lift coefficient of the airfoil.

Drag Results

The drag results can be seen by observing the section total drag coefficient verses angle of attack curves presented in Figures 25 through 30. Figure 25 shows that when blowing was applied to the model without the splitter plate, the section total drag coefficient increased. However, the increase was mainly due to the momentum coefficient. The section profile drag coefficient was about the same with and without blowing. Figure 26 shows that when the splitter plate was attached to the model and no blowing applied, the section total drag coefficient increased. As the chord length of the splitter plate increased so did the section total drag coefficient.

When blowing was applied to the three model configurations with the splitter plates the section total drag coefficient actually decreased or remained the same as the section total drag coefficient of the particular model without blowing. Figure 27 shows that when blowing was applied to the model with the 1.5 inch splitter plate chord, the section total drag coefficient actually decreased. Figures 28 and 29 show that blowing on the models with the 1.0 inch splitter plate chord and the 0.5 inch splitter plate chord caused the total drag coefficient to remain essentially the same as the total drag coefficient without blowing. However, on all three model configurations with the splitter plate and blowing, the profile drag coefficient decreased since the momentum coefficient contributed to

the total drag coefficient. The decrease in the profile drag coefficient was a result of the decrease in the pressure drag coefficient.

Figure 30 shows that while the total drag coefficient did not always decrease at the higher momentum coefficients when the three different splitter plates were attached to the model, the profile drag coefficient always decreased. In fact, some negative coefficients of profile drag were observed at the higher momentum coefficients shown in Figure 30. However, the section total drag coefficients were always positive when the momentum coefficient was added to the profile drag coefficient. This indicates that the splitter plate on all three models effectively reduced the profile drag on the airfoil by reducing the mixing losses.

Lift-to-Drag Ratio Results

The lift-to-drag ratio results are presented in Figures 31 through 36. Figure 31 shows that the model without the splitter plate had a larger lift-to-drag ratio at negative angles of attack when blowing was applied compared to the lift-to-drag ratio when there was no blowing. This occurred because the airfoil had positive lift coefficients at negative angles of attack when blowing was applied. However, the lift-to-drag ratio of the model without blowing steadily increased until it was essentially the same as the model with blowing at positive angles of attack.

When the three different splitter plates were attached to the model and blowing applied, the lift-to-drag ratios were larger than the lift-to-drag ratios of the model with blowing but without the splitter plate. Figure 32 shows the increase in the lift-to-drag ratios due to the splitter plate with blowing. Yet, when the blowing was stopped on the four models, the lift-to-drag ratios were larger for the three models with the splitter plates compared to the model without a splitter plate at negative angles of attack. This was due to the fact that the three models with the splitter plates had positive lift coefficients at negative angles of attack. The lift-to-drag ratios of the model without the splitter plate steadily increased until they were essentially the same as the lift-to-drag ratios of the models with the splitter plates. This occurred at positive angles of attack. Figure 33 shows the change in the lift-to-drag ratio due to the splitter plate.

The advantage of the splitter plate in increasing the lift-to-drag ratio was evident when blowing was applied to the airfoil. Figure 34 shows that at higher momentum coefficients, the three models with the splitter plates had higher lift-to-drag ratios than the model without the splitter plate at similar momentum coefficients. In fact, two of the models with the splitter plates obtained lift-to-drag ratios higher than the model without the splitter plate even though their momentum coefficients were lower than the model without the splitter plate. Figure 35 shows

the lift-to-drag ratio increased due to the 1.5 inch splitter plate chord even though the model without the splitter plate had a larger momentum coefficient. Also, Figure 36 shows the lift-to-drag ratio increased due to the 1.0 inch splitter plate chord even though the model without the splitter plate had a larger momentum coefficient. Thus the models with the splitter plates and blowing obtained larger lift-to-drag ratios than the model with blowing, but without the splitter plate.

Comparison of Results with Previous Work

The results obtained by Kind compared favorably with the lift-to-drag ratios contained in Figures 31 through 36. Kind obtained an overall lift-to-drag ratio of 30:1 without a splitter plate using the same procedures to compute the section total drag coefficient. This ratio is about the same that was obtained on the current model with and without blowing at slightly positive angles of attack.

Kind had a lift-to-drag ratio of approximately 42:1 with a splitter plate attached to his airfoil and rotated 45 degrees from the chordline. However, lift-to-drag ratios as high as 50:1 were observed in this study at angles of attack equal to one and two degrees.

Comparison of the Three Splitter Plates

Since the drag data contained some scatter, an accurate evaluation of the most effective of the three splitter plates was not possible. However, trends were observed.

First, the longest of the three plates consistently attained a higher section lift coefficient under nearly identical test conditions. Second, the two longer plates seemed to aid the effectiveness of the blowing air at low momentum coefficients. Finally, the lift-to-drag ratios of the three models with the splitter plates were essentially the same.

VII. Conclusions

The following conclusions were formed as a result of the two-dimensional wind tunnel study on a circulation controlled airfoil with splitter plate.

1. The splitter plate increases the section lift-to-total drag ratio on a circulation controlled airfoil.
2. The splitter plate increases the section lift coefficient on a circulation controlled airfoil.
3. The splitter plate decreases the section profile drag coefficient on a circulation controlled airfoil.
4. The section lift coefficient increases as the chord length of the splitter plate increases on a circulation controlled airfoil.
5. The decrease in the section lift coefficient at separation is not as large on a circulation controlled airfoil with a splitter plate as it is without a splitter plate.

VIII. Recommendations

The results of the wind tunnel tests on the circulation controlled airfoil with a splitter plate revealed that modifications to the model and apparatus should be made. Also, further tests are necessary to determine the effect of splitter plates on the lift-to-drag ratios on circulation controlled devices.

It is recommended that the model airfoil and apparatus be improved by:

1. Constructing a wake survey rake on which the majority of the total head probes of the rake are concentrated in the lower half of the tunnel test section.
2. Roughening the surface of the airfoil so the flow over the model will be turbulent during wind tunnel tests.

It is recommended that further wind tunnel tests and analytical work include:

1. The effect on the section lift-to-drag ratio of varying the angle between the splitter plate chordline and the airfoil chordline.
2. The effect on the section lift-to-drag ratio of varying the location of the splitter plate along the airfoil chordline.
3. The effect of the splitter plate on the section characteristics at higher momentum coefficients.

4. Investigating the contribution of the various types of drag such as pressure and viscous drag on circulation control devices with and without splitter plates.
5. The effect of changing the splitter plate chord length on the section characteristics of the airfoil.

Bibliography

1. American Society of Mechanical Engineers Research Committee on Fluid Meters. Flowmeter Computation Handbook. New York: American Society of Mechanical Engineers, 1961.

2. Anscombe, A. and J. Williams. "Some Comments on High-Lift Testing in Wind Tunnels with Particular Reference to Jet-Blowing Models." Journal of the Royal Aeronautical Society, 61:529-540 (August 1957).

3. Englar, R. J. Two-Dimensional Subsonic Wind Tunnel Tests of Two 15-Percent Thick Circulation Control Airfoils. NSRDC Technical Note AL-211. Bethesda, Maryland: Naval Ship Research and Development Center, August 1971. AD 900210.

4. Karamcheti, K. Principles of Ideal-Fluid Aerodynamics. New York: John Wiley and Sons, Inc., 1966.

5. Kind, R. J. A Proposed Method of Circulation Control. Unpublished dissertation. University of Cambridge: Aeronautical Engineering Department, 1967.

6. Lachmann, G. V., editor. Boundary Layer and Flow Control. Vol. I. New York: Pergamon Press, 1961.

7. Ness, N. "Downwash Correction for a Two-Dimensional Finite Wing." Journal of Aircraft, 8:745-746 (September 1971).

8. Pankhurst, R. C. and D. W. Holder. Wind-Tunnel Technique. London: Sir Isaac Pitman and Sons, Ltd., 1952.

9. Patrick, R. P. Effect of Flap Blowing on the Sectional Characteristics of an NACA 0015 Airfoil. Unpublished thesis. Wright-Patterson Air Force Base, Ohio: Air Force Institute of Technology, March 1965.

10. Pope, A. Wind-Tunnel Testing (Second Edition). New York: John Wiley and Sons, Inc., 1961.

11. Schlichting, H. Boundary-Layer Theory (Sixth Edition). New York: McGraw-Hill Book Co., 1968.

12. Stearns, R. F., et al. Flow Measurement with Orifice Meters. New York: D. Van Nostrand Co., Inc., 1951.

13. Walters, R. E., et al. Circulation Control by Steady and Pulsed Blowing for a Cambered Elliptical Airfoil. NR 215-163. Morgantown, West Va: West Virginia University, July 1972. AD 751045.

14. Williams, R. M. and H. J. Harvey. Two Dimensional Subsonic Wind Tunnel Tests on a 20 Percent Thick, 5 Percent Cambered Circulation Control Airfoil. NSRDC Technical Note AL-176. Washington, D. C.: Naval Ship Research and Development Center, 1970. AD 877764.

Appendix A

Tabulated Data

Table I

The Location of the Static Pressure Taps on the Upper Surface of the Airfoil

Pressure Tap	$\frac{x}{c}$	$\frac{y}{c}$
0	0	0
U-1	.0066	.0243
U-2	.0182	.0401
U-3	.0355	.0551
U-4	.0582	.0702
U-5	.0716	.0773
U-6	.0862	.0841
U-7	.1020	.0908
U-8	.1562	.1089
U-9	.1975	.1194
U-10	.2422	.1285
U-11	.2900	.1361
U-12	.3925	.1465
U-13	.5000	.1500
U-14	.6074	.1465
U-15	.7099	.1361
U-16	.8026	.1194
U-17	.8439	.1089
U-18	.8981	.0908
U-19	.9284	.0773
U-20	.9818	.0401
U-21	.9934	.0243
22	1.0000	0
U-19L	.9284	.0773
U-19R	.9284	.0773
U-20L	.9818	.0401
U-20R	.9818	.0401

L - The pressure tap is located 6 in. to the left of the airfoil center span.

R - The pressure tap is located 6 in. to the right of the airfoil center span.

Table II

The Location of the Static Pressure Taps
on the Lower Surface of the Airfoil

Pressure Tap	$\frac{x}{c}$	$\frac{y}{c}$
0	0	0
L-1	.0066	-.0081
L-2	.0182	-.0134
L-3	.0355	-.0185
L-4	.0582	-.0234
L-5	.0716	-.0258
L-6	.0862	-.0280
L-7	.1020	-.0302
L-8	.1562	-.0363
L-9	.1975	-.0398
L-10	.2422	-.0428
L-11	.2900	-.0454
L-12	.3925	-.0488
L-13	.5000	-.0500
L-14	.6574	-.0475
L-15	.7099	-.0454
L-16	.8026	-.0398
L-17	.8439	-.0363
L-18	.9418	-.0234
L-19	.9645	-.0185
L-20	.9818	-.0134
L-21	.9934	-.0081
22	1.0000	0

Table III

The Spanwise Slot Total Pressure Distribution for Various Momentum Coefficients

C_μ	.012	.015	.02	.023
Z in.	P_t in. H_2O (gauge)	P_t in. H_2O (gauge)	P_t in. H_2O (gauge)	P_t in. H_2O (gauge)
0	17.0	27.0	2.0	2.5
1	17.0	27.0	2.3	2.7
2	17.0	26.9	2.3	2.7
3	17.0	27.0	2.3	2.7
4	17.1	27.0	2.3	2.7
5	17.3	26.5	2.3	2.7
6	17.3	26.6	2.3	2.7
7	17.6	26.7	2.3	2.7
8	18.0	26.9	2.3	2.7
9	18.2	27.0	2.3	2.7
10	18.2	27.0	2.4	2.7
11	18.2	27.0	2.4	2.7
12	18.3	26.8	2.4	2.7
13	18.5	26.4	2.4	2.7
14	18.5	26.4	2.4	2.8
15	18.6	26.6	2.4	2.8
16	18.7	26.4	2.4	2.7
17	19.0	26.5	2.4	2.8
18	18.9	27.3	2.4	2.7
19	19.0	27.1	2.4	2.8
20	19.1	27.1	2.4	2.9
21	19.3	27.2	2.4	2.8
22	19.3	26.9	2.4	2.9
23	19.3	26.8	2.4	2.8
24	19.3	26.8	2.4	2.9
25	19.2	26.7	2.4	2.9
26	17.1	26.2	2.4	2.9

Z - The distance from the left endplate in inches.

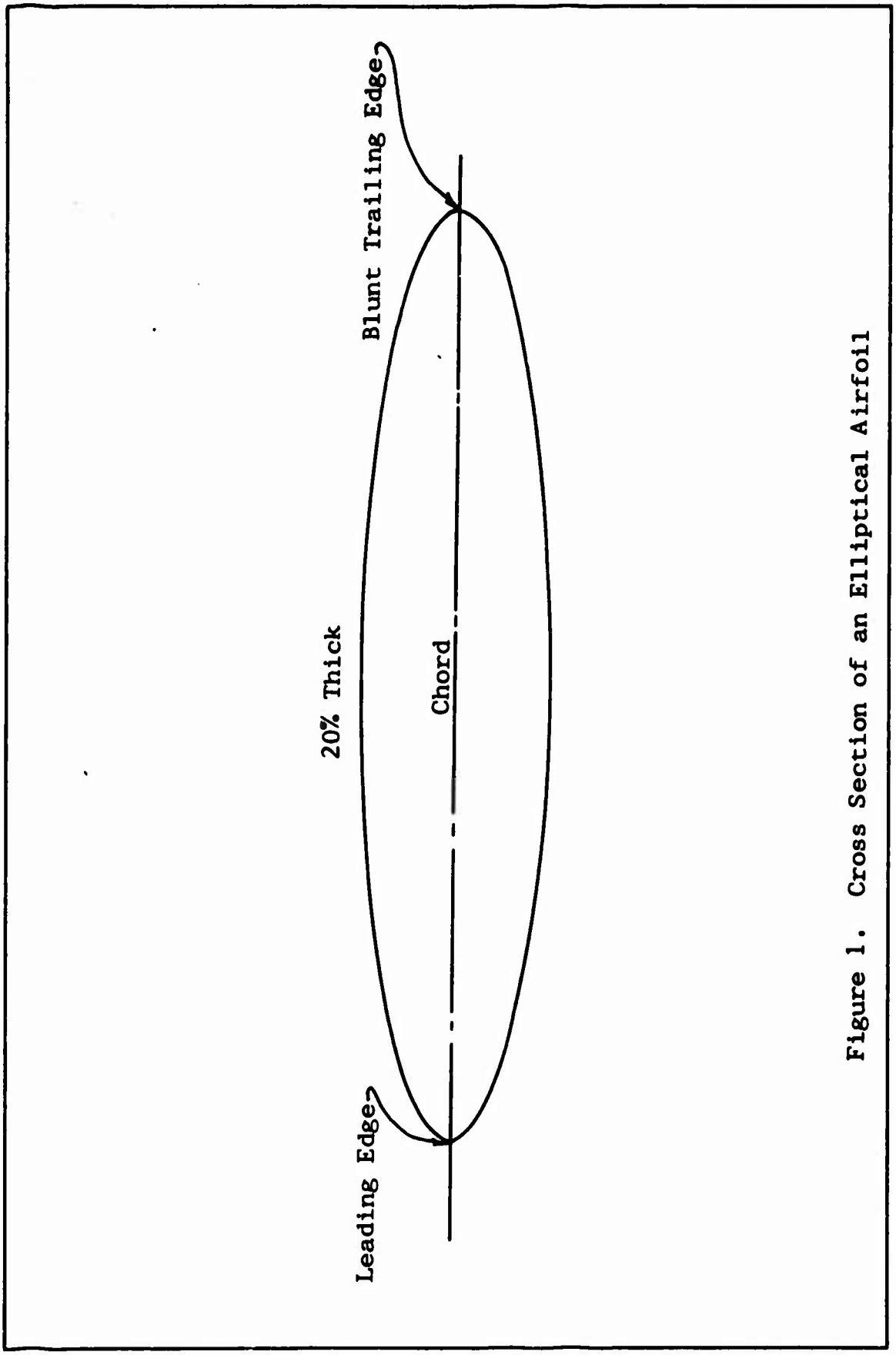

Figure 1. Cross Section of an Elliptical Airfoil

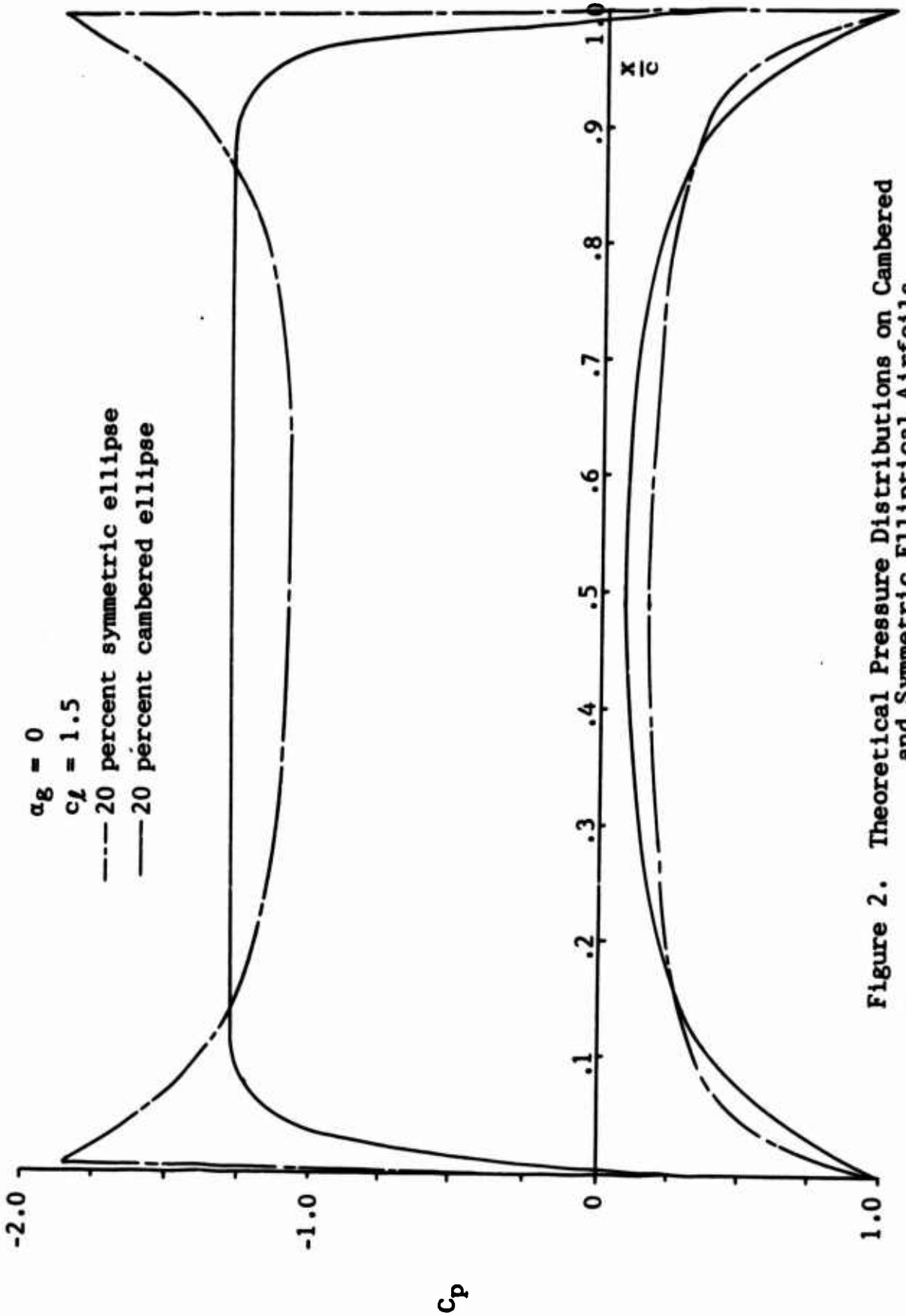

Figure 2. Theoretical Pressure Distributions on Cambered and Symmetric Elliptical Airfoils

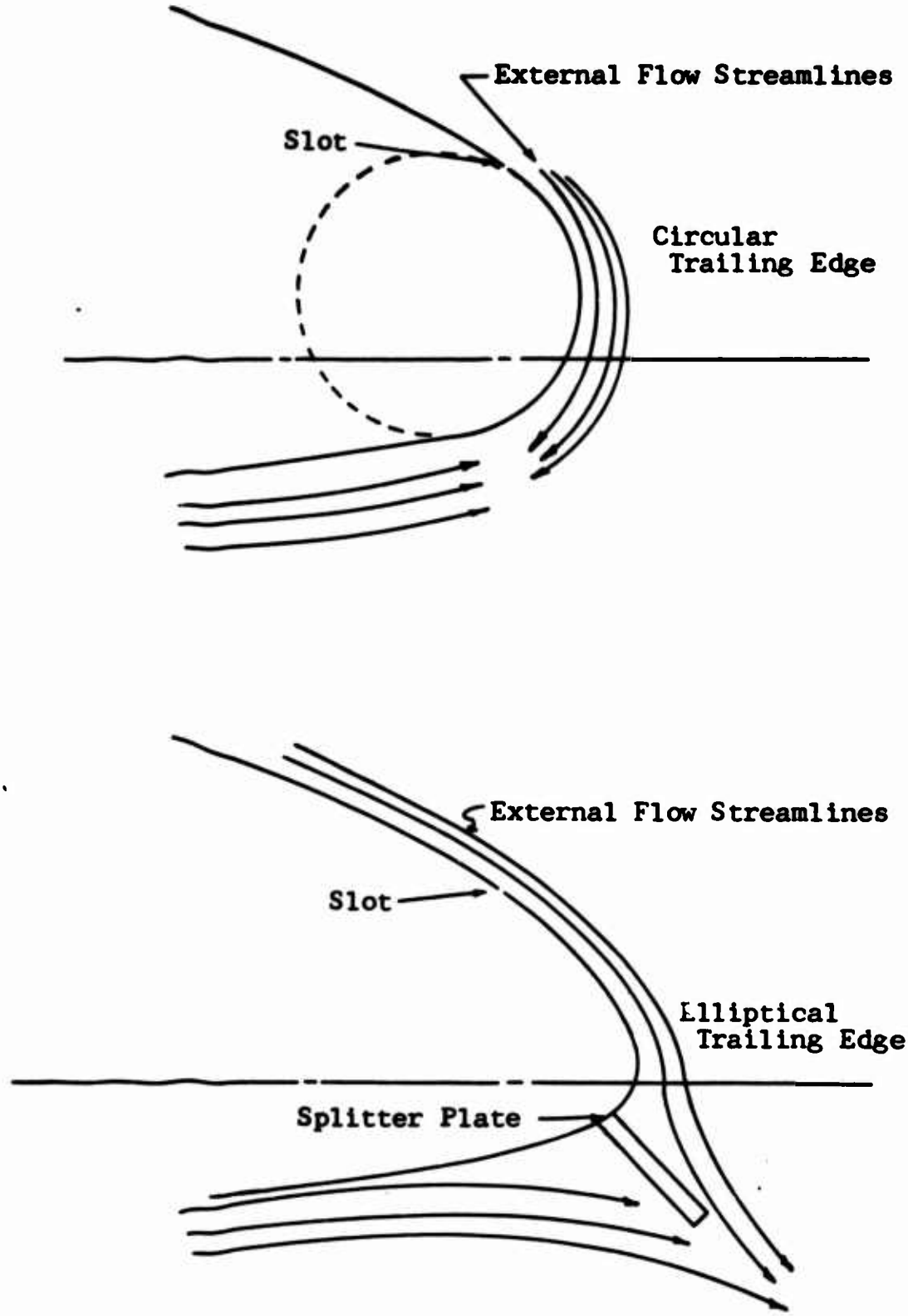

Figure 3. Comparison of the Air Flow on a Circular Trailing Edge with the Air Flow on a Pure Ellipse Trailing Edge

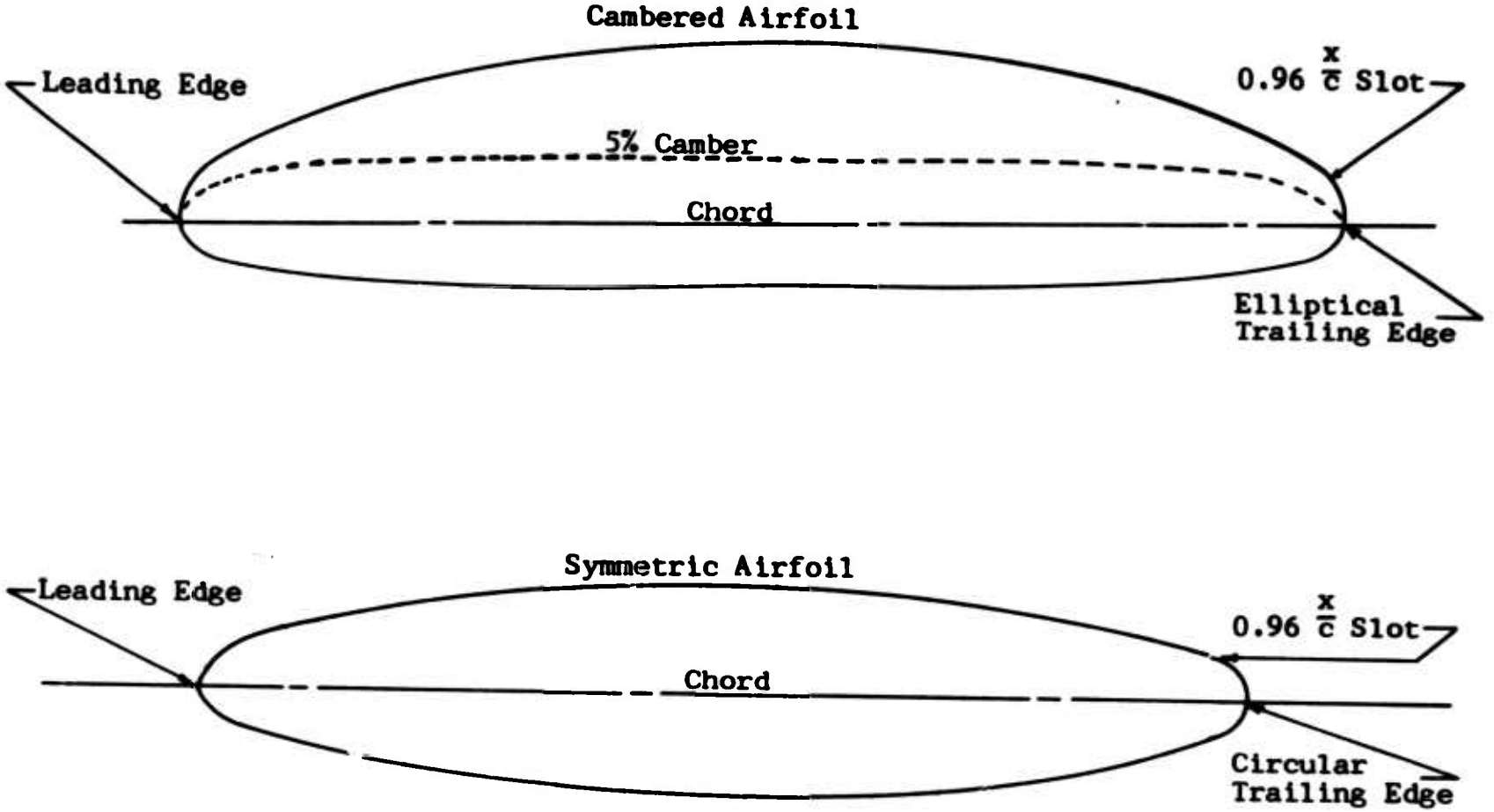

Figure 4. Comparison of the Cross Sections of a Symmetric Elliptical Airfoil with a Cambered Elliptical Airfoil

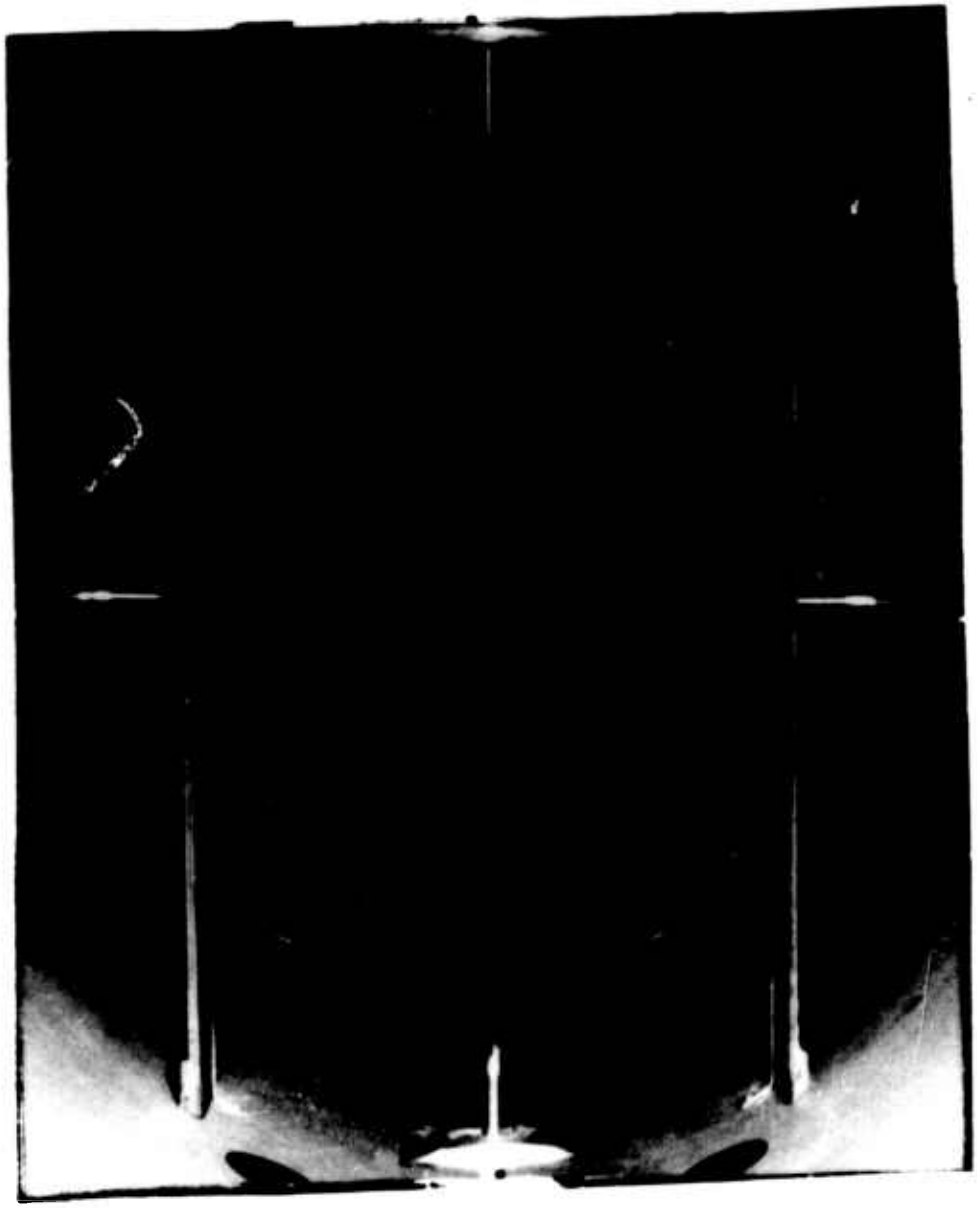

Figure 5. Front View of Test Section

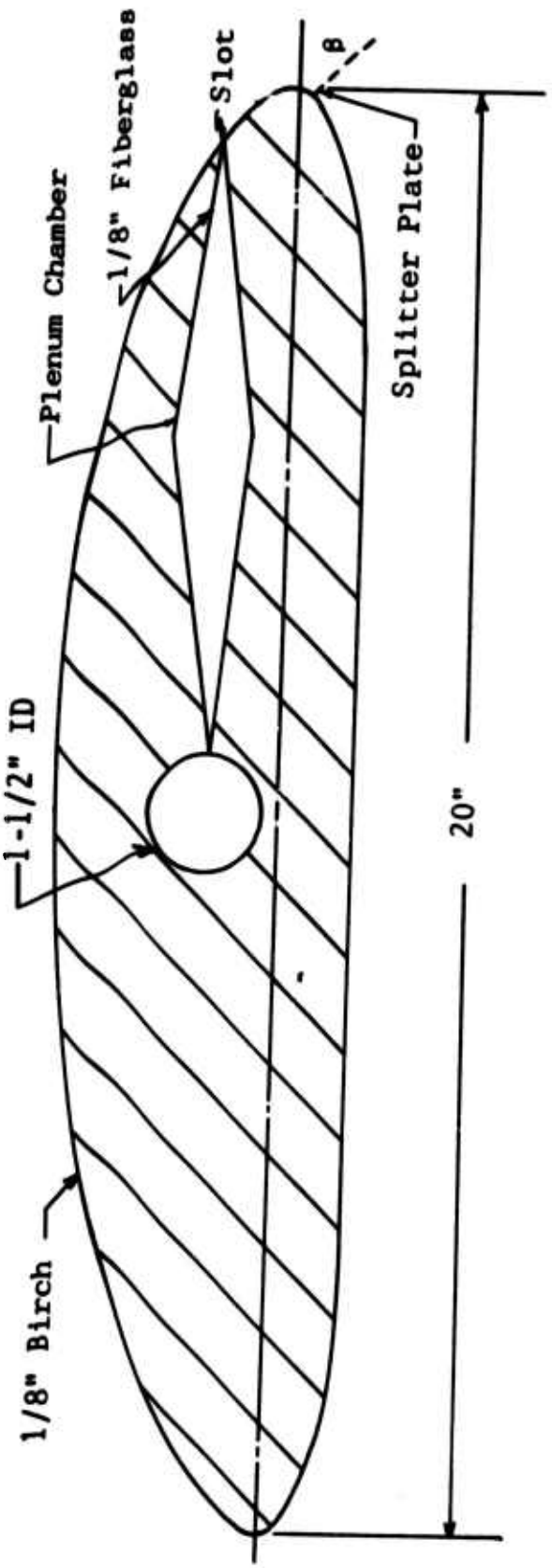

Figure 6. Cross Section of Airfoil Model

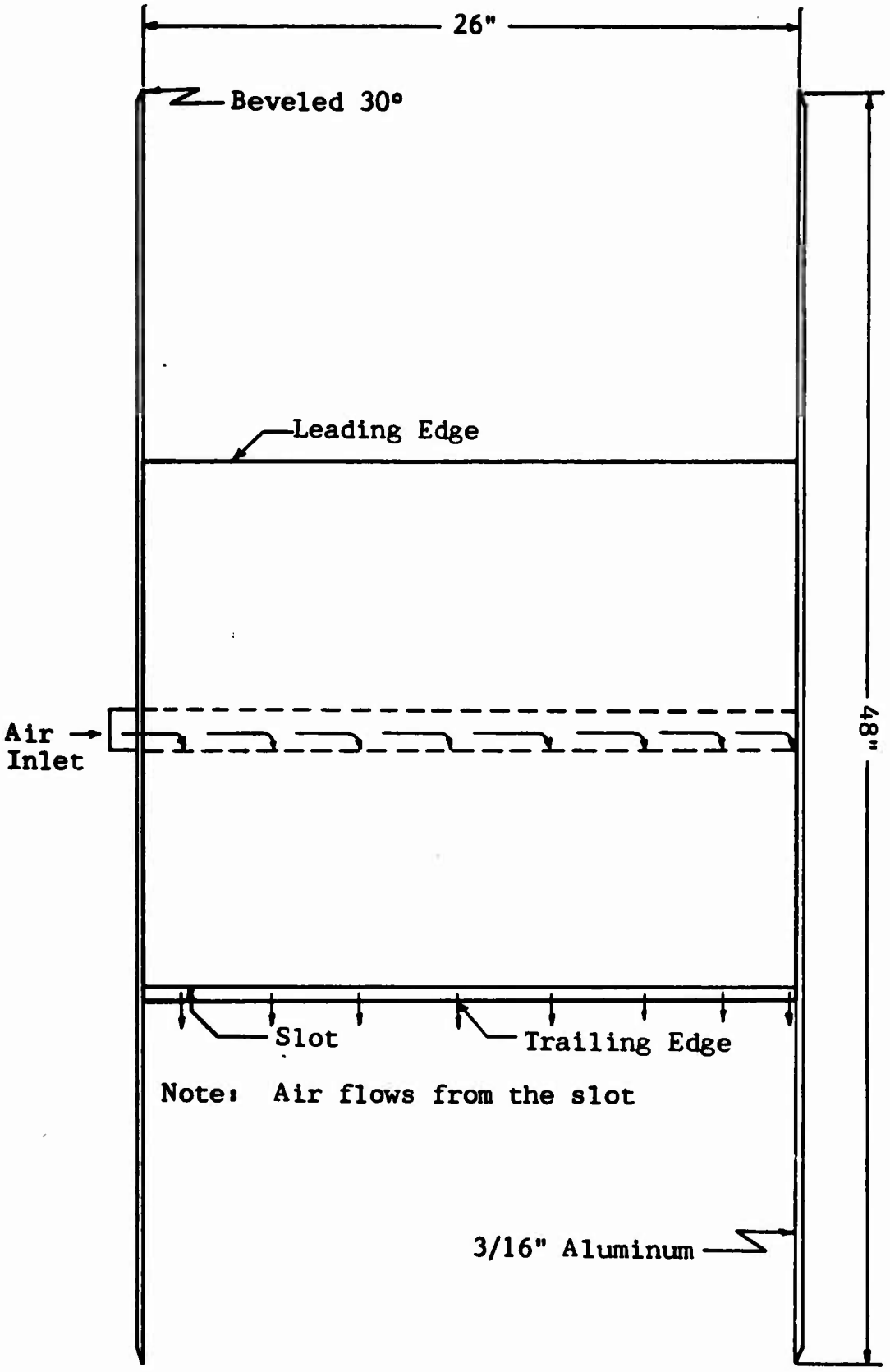

Figure 7. Top View of Model and Blowing Air Flow

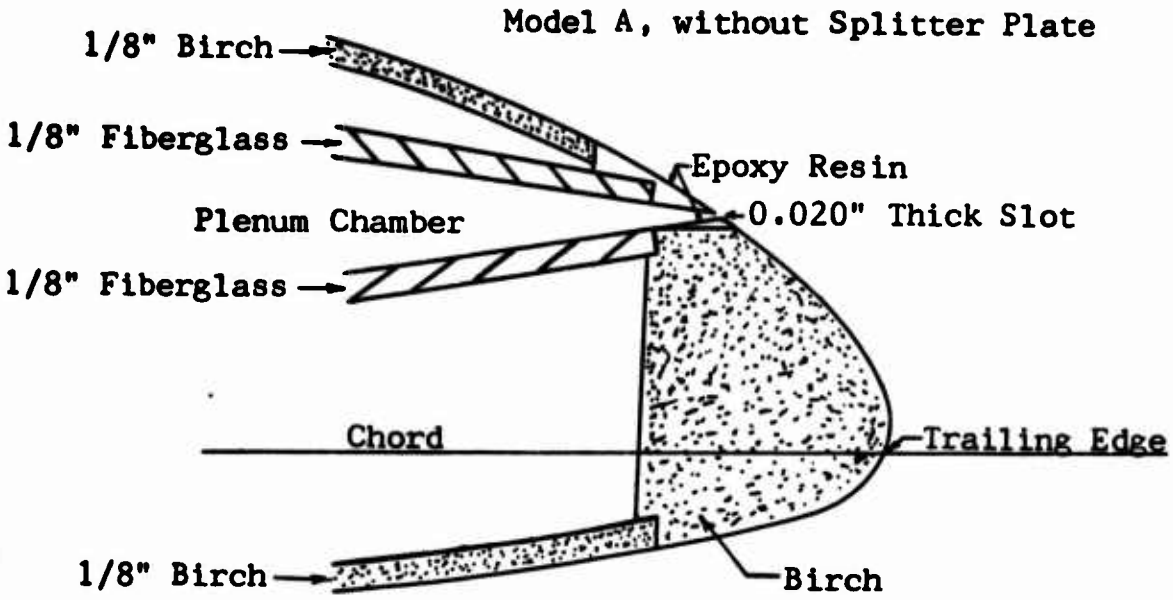

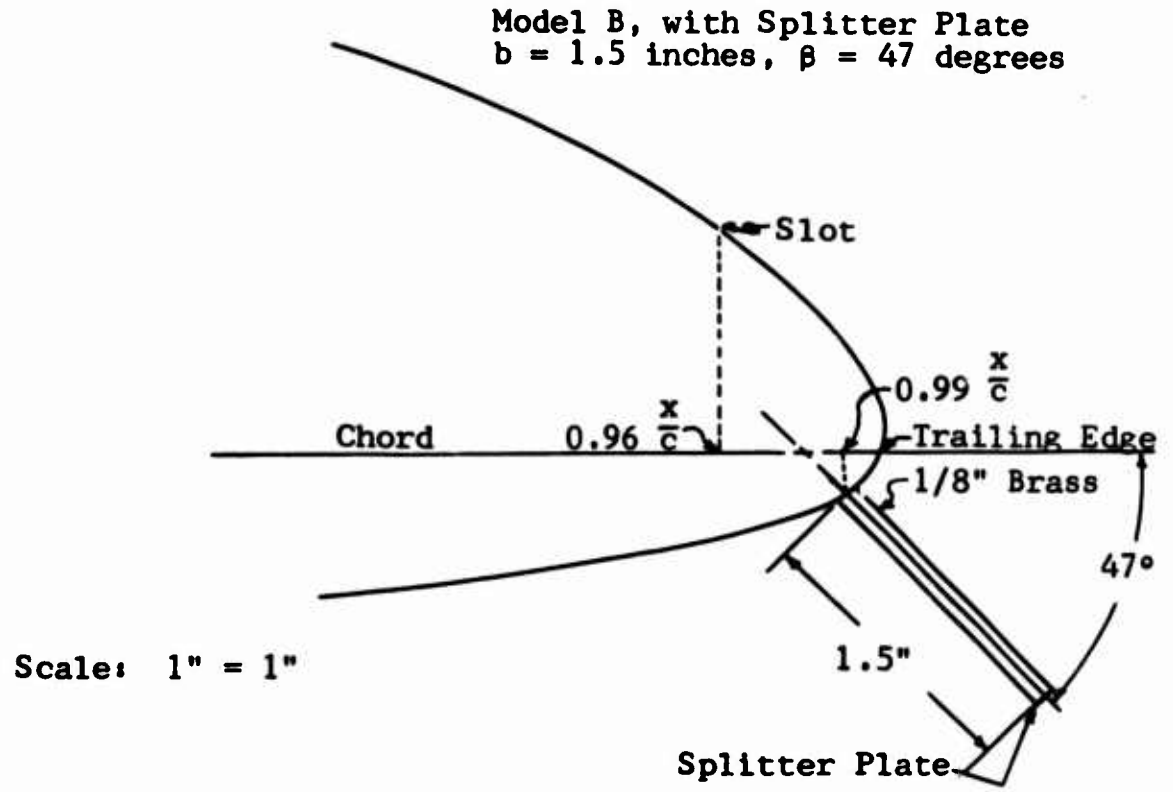

Figure 8. The Slot and Trailing Edge Configurations of Model A and Model B

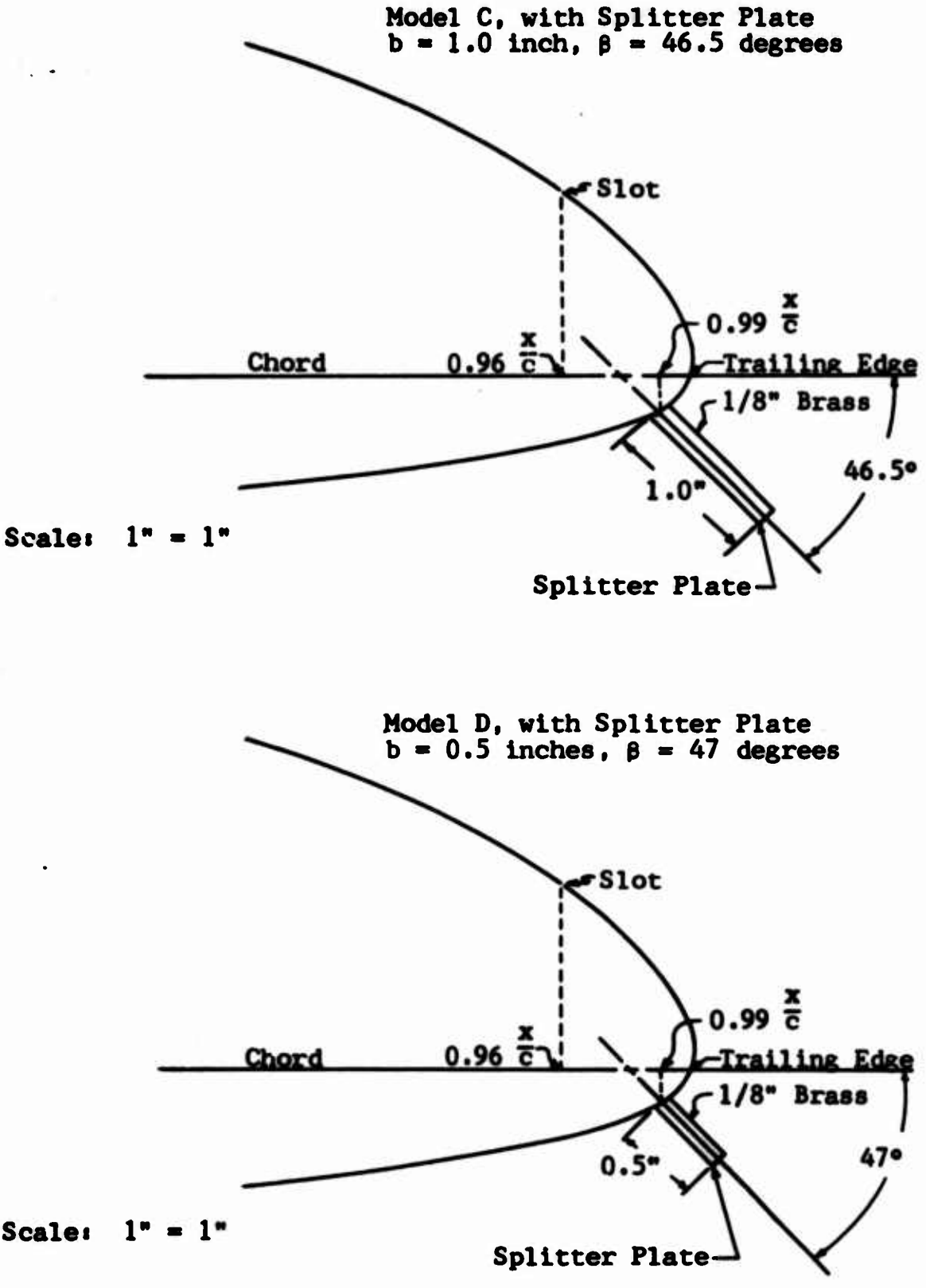

Figure 9. The Trailing Edge Configurations of Model C and Model D

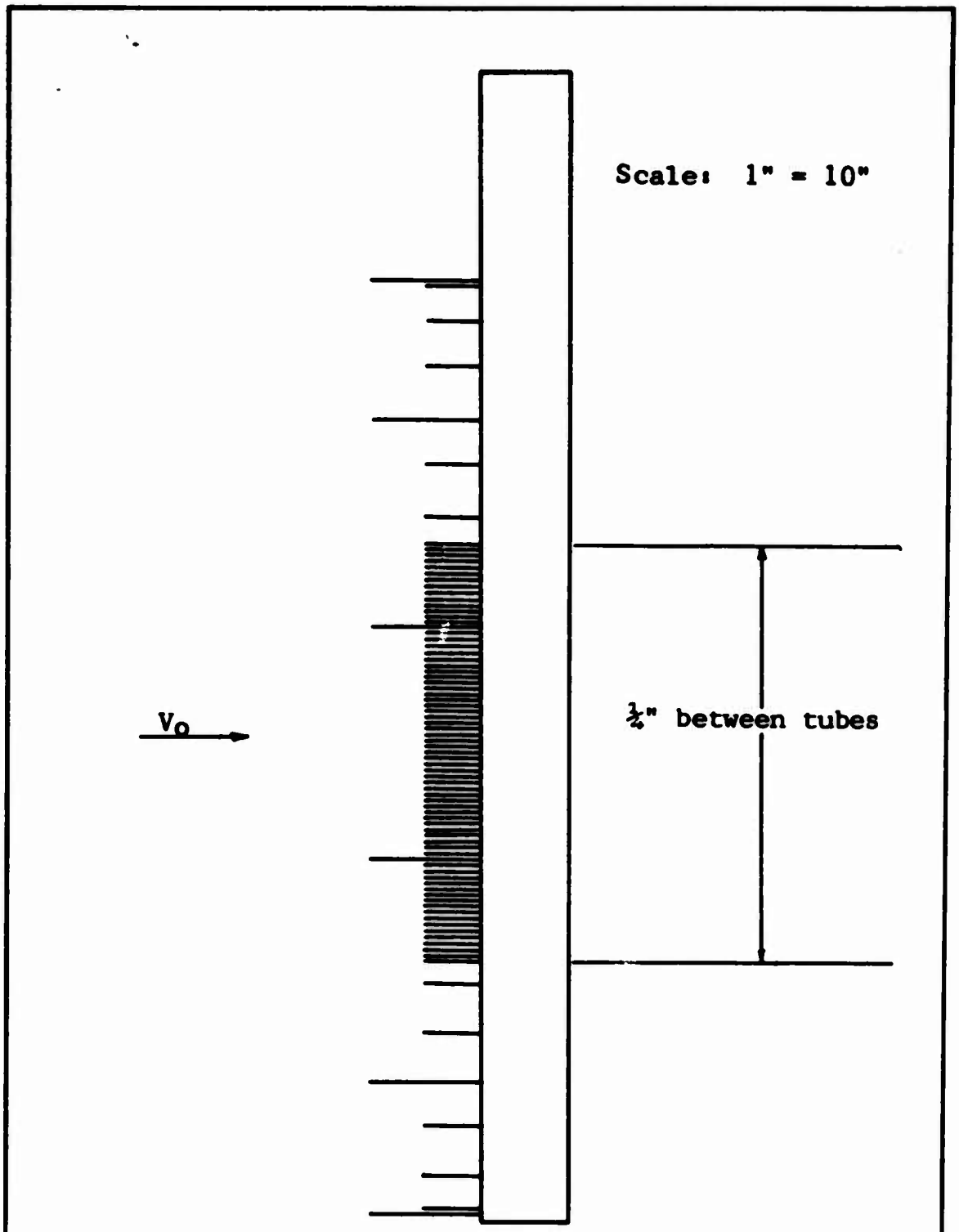

Figure 10. Wake Survey Rake

(Ref 9)

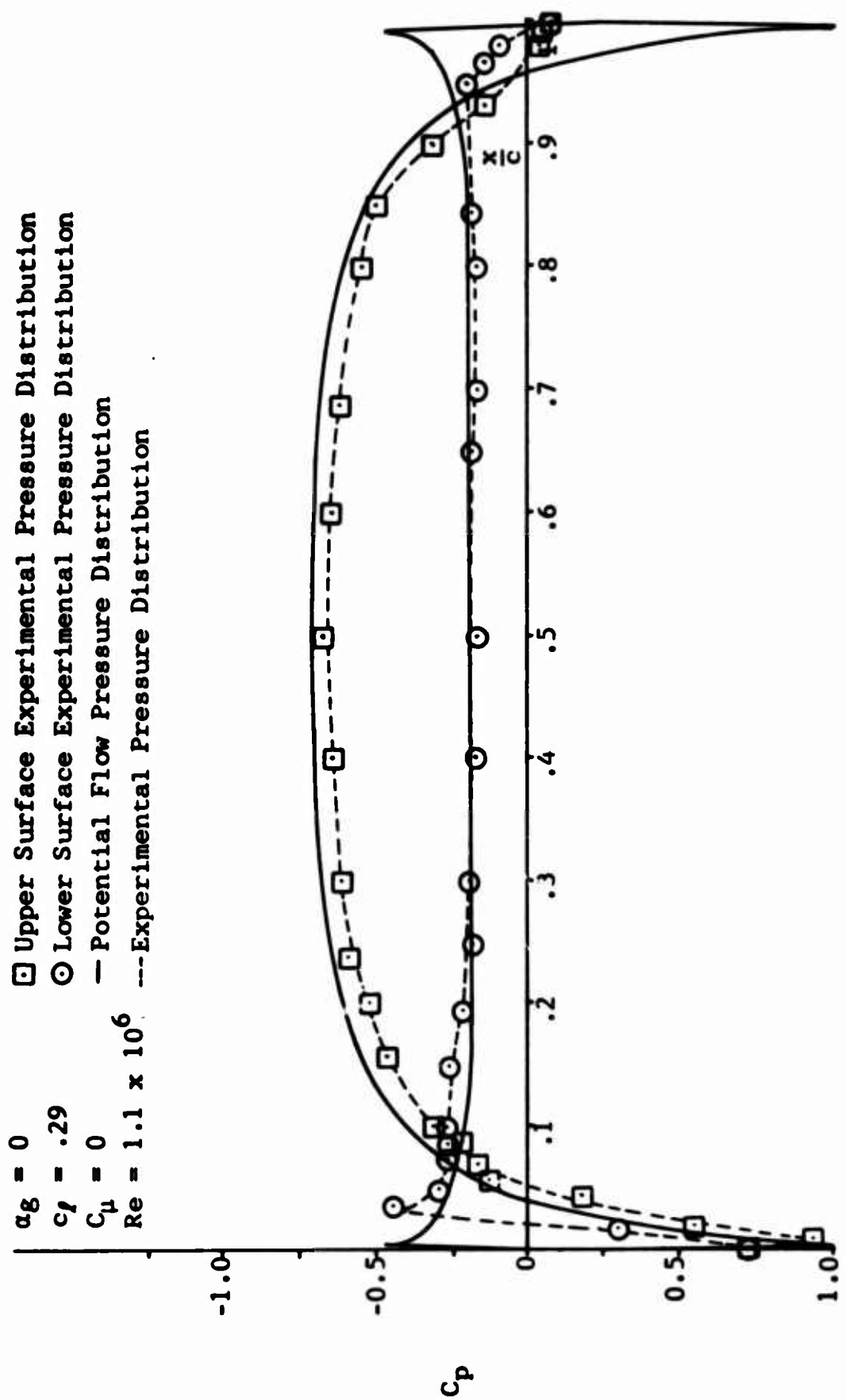

Figure 11. Experimental and Potential Flow Pressure Distributions on Model A, Without Splitter Plate

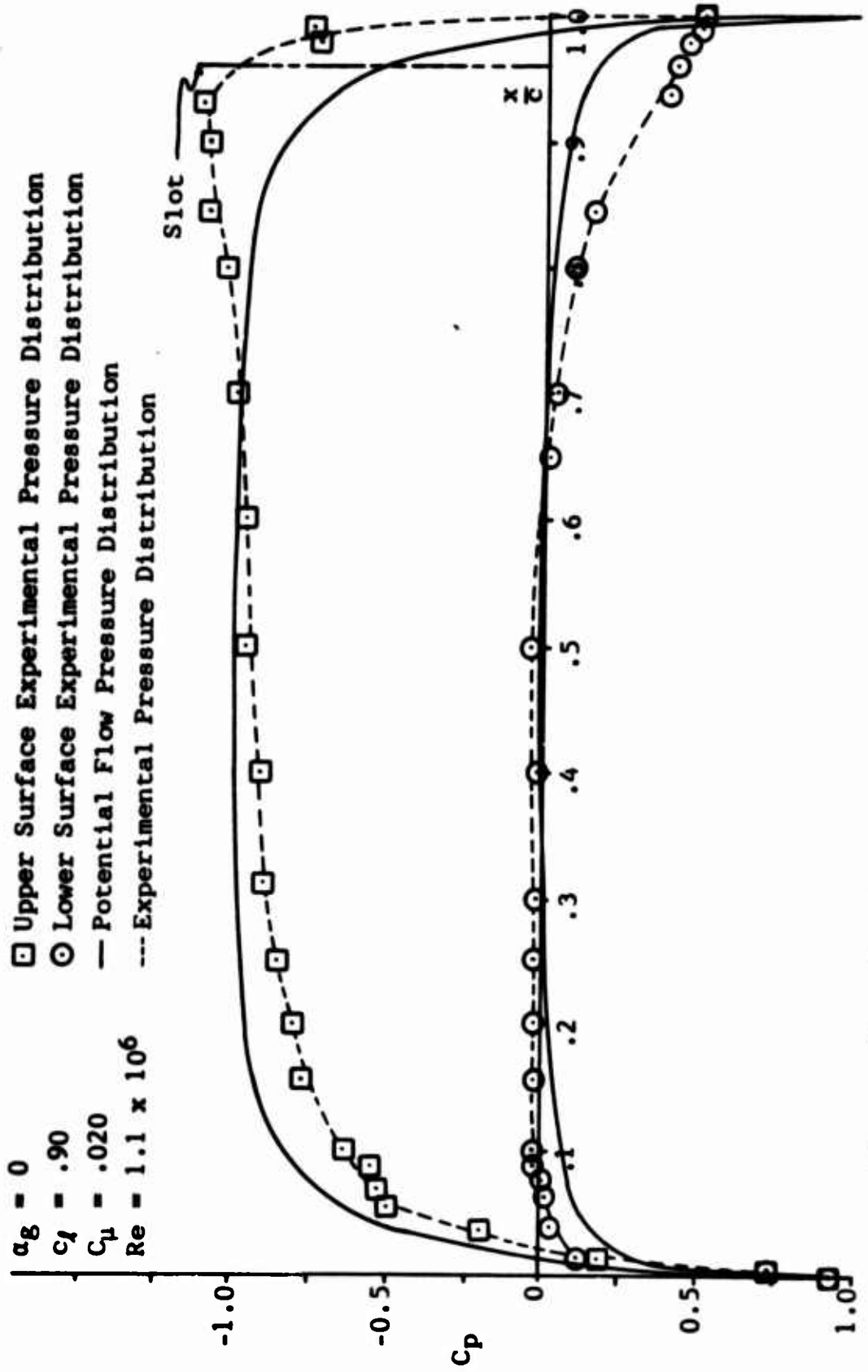

Figure 12. Experimental and Potential Flow Pressure Distributions on Model A, Without Splitter Plate

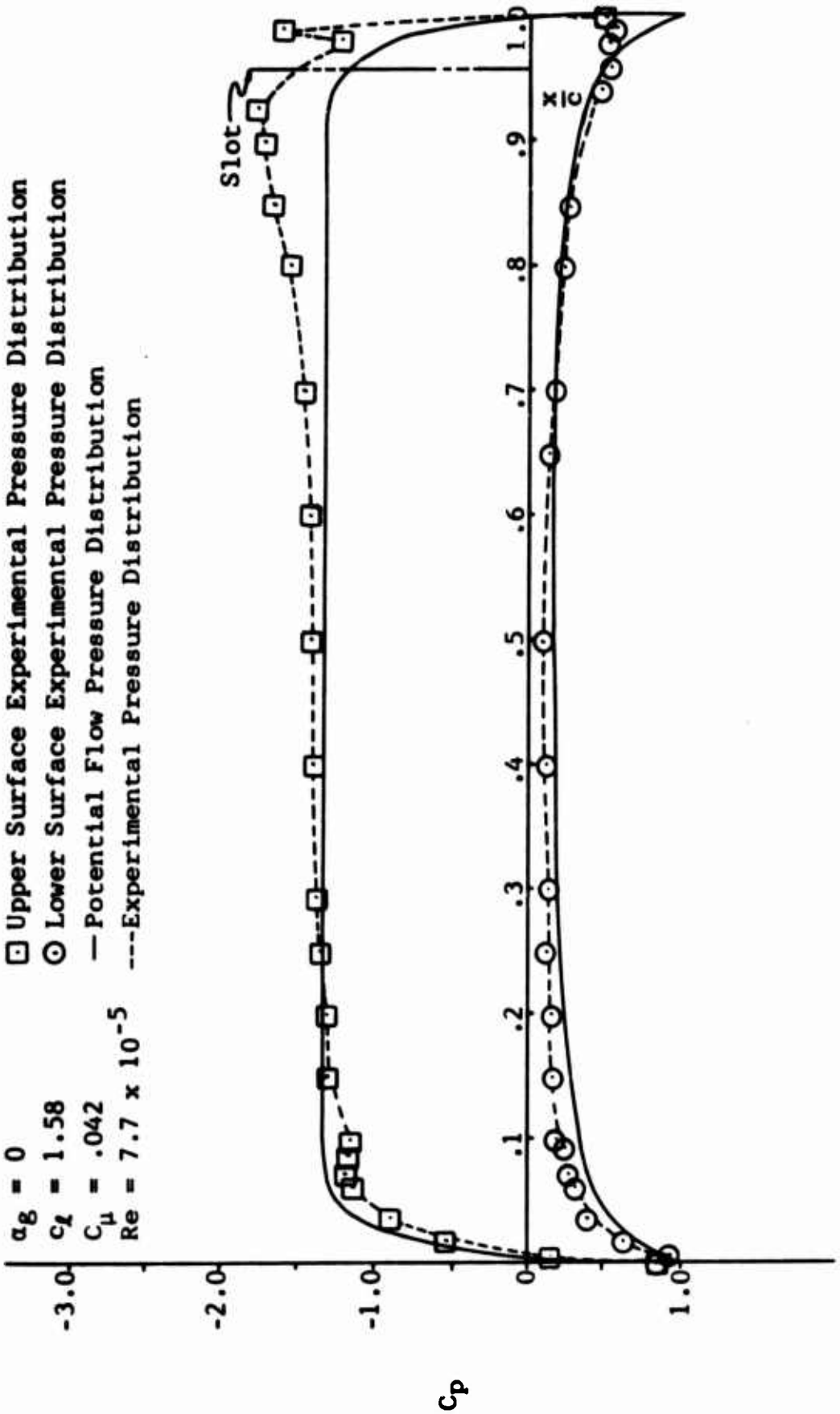

Figure 13. Experimental and Potential Flow Pressure Distributions on Model A, Without Splitter Plate

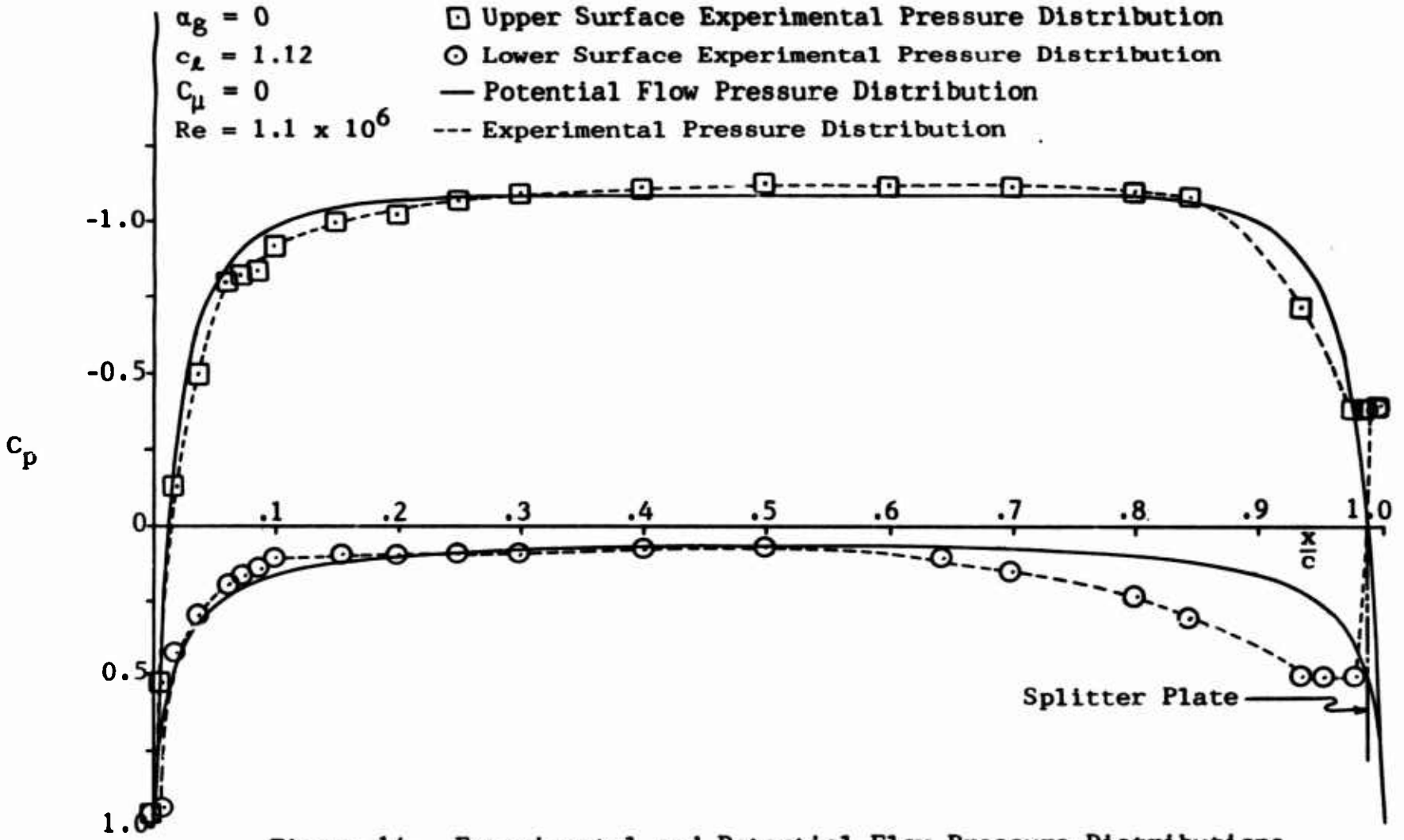

Figure 14. Experimental and Potential Flow Pressure Distributions on Model B, with Splitter Plate, b = 1.5 inches

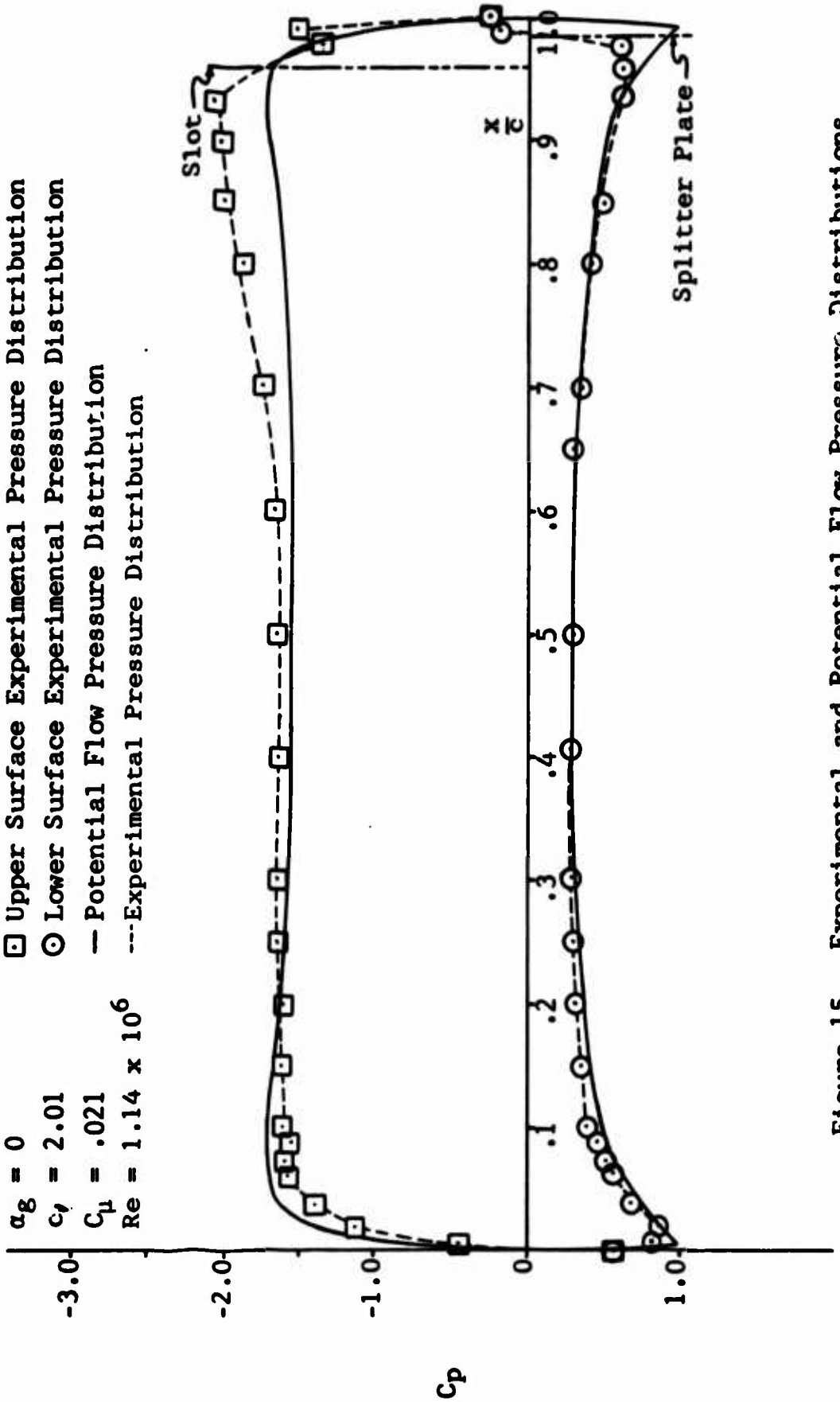

Figure 15. Experimental and Potential Flow Pressure Distributions on Model B, with Splitter Plate, b = 1.5 inches

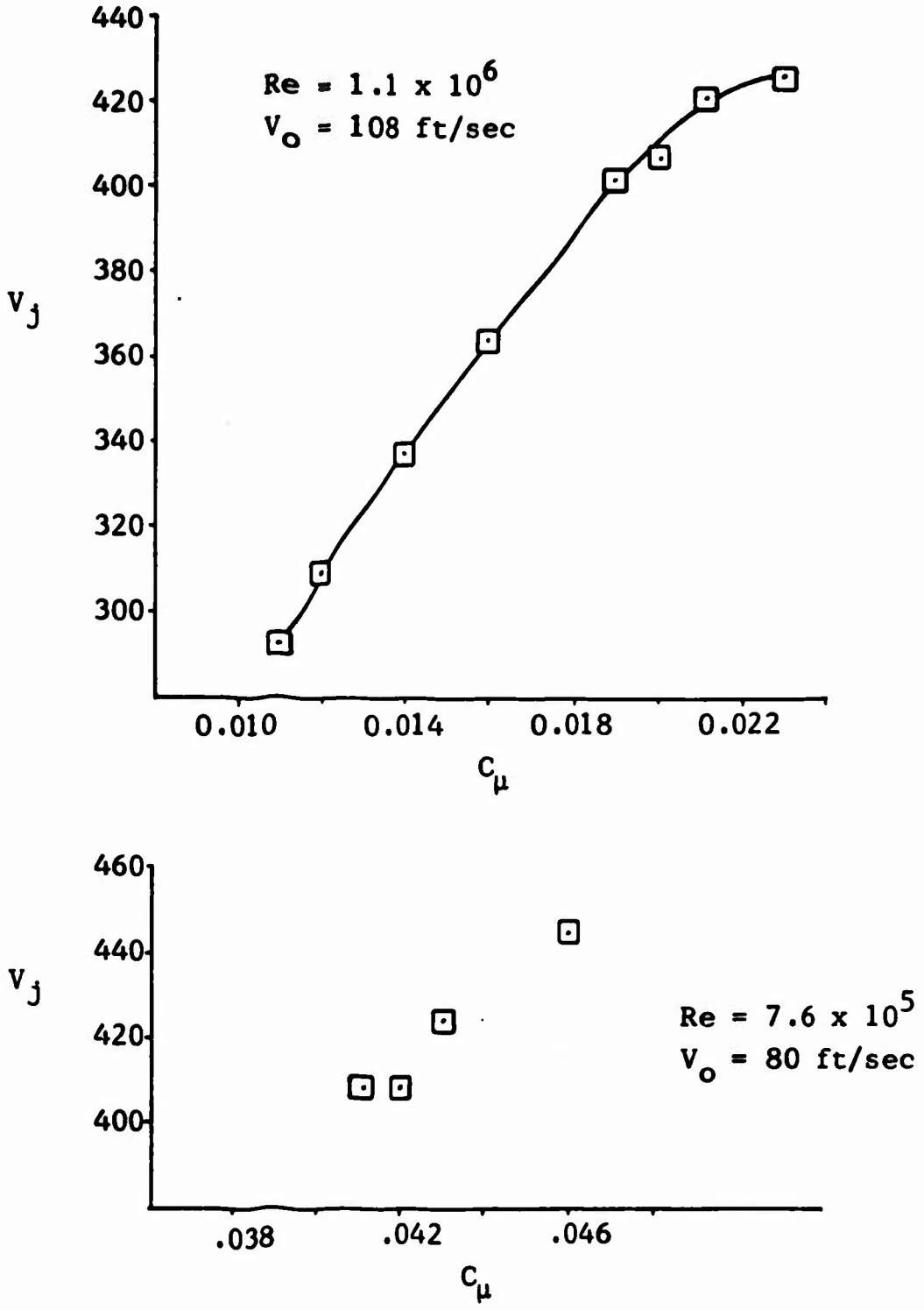

Figure 16. Velocity at the Slot for Various Momentum Coefficients

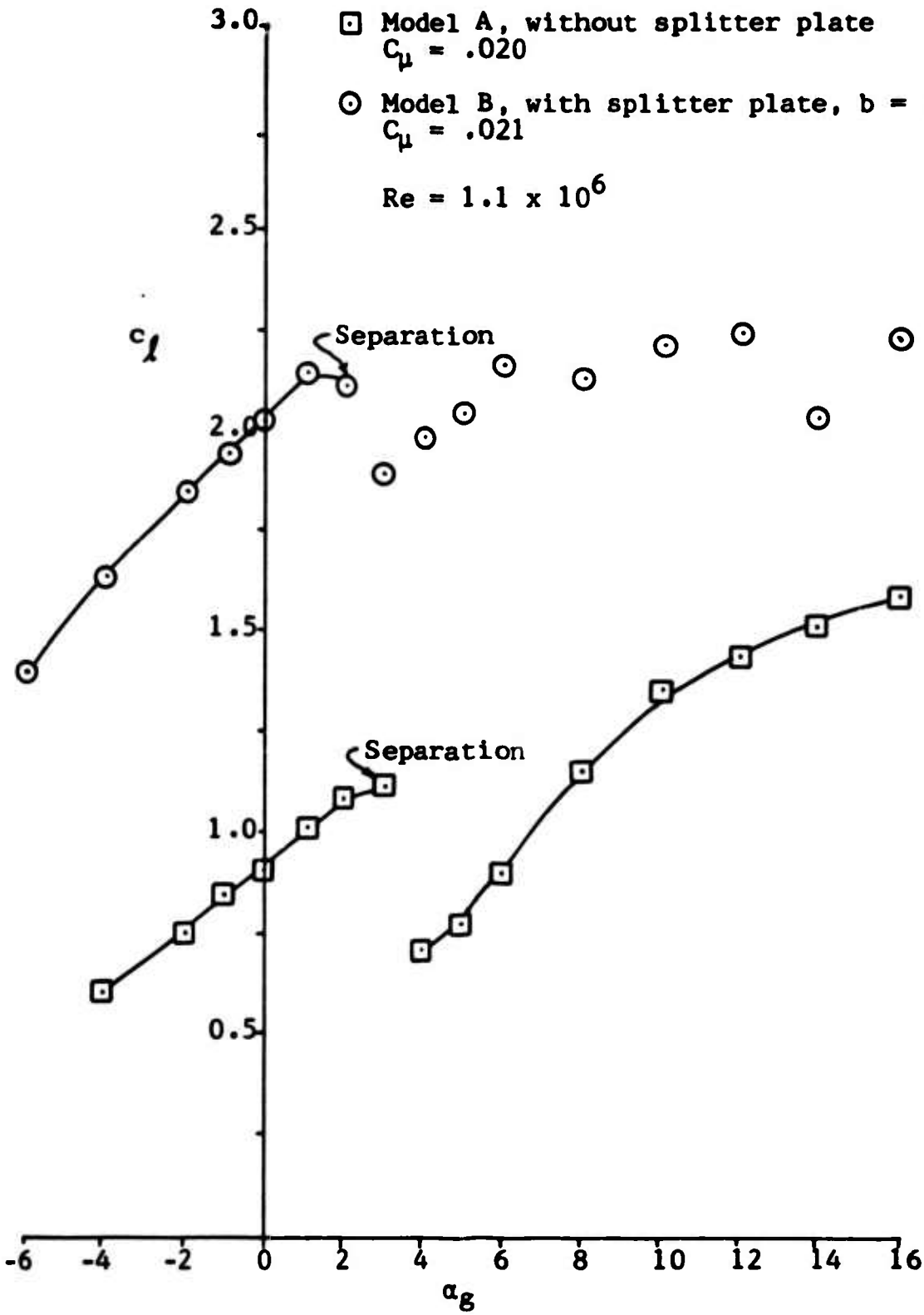

Figure 17. The Effect of Separation on c_ℓ vs α_g

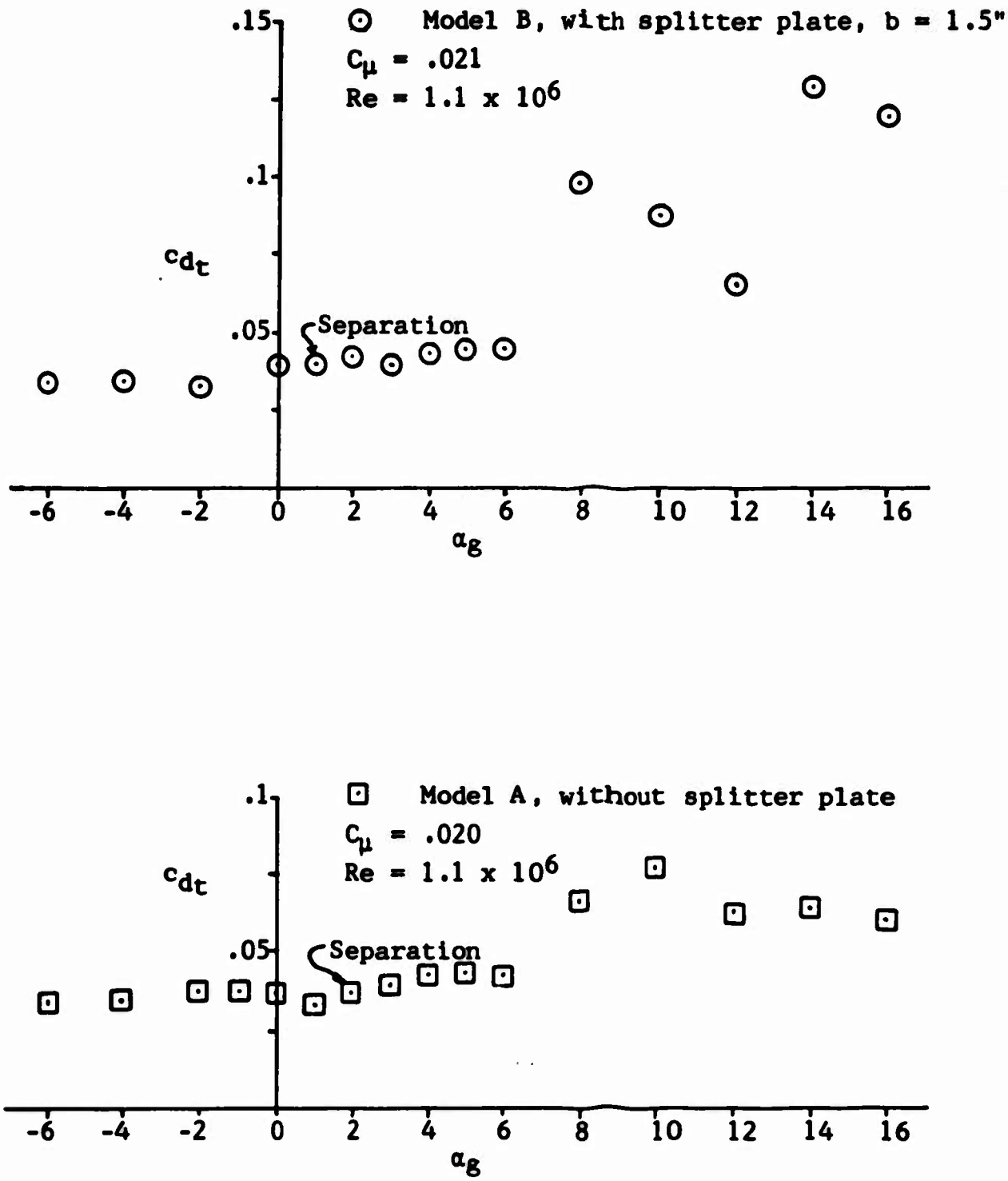

Figure 18. The Effect of Separation on c_{d_t} vs α_g

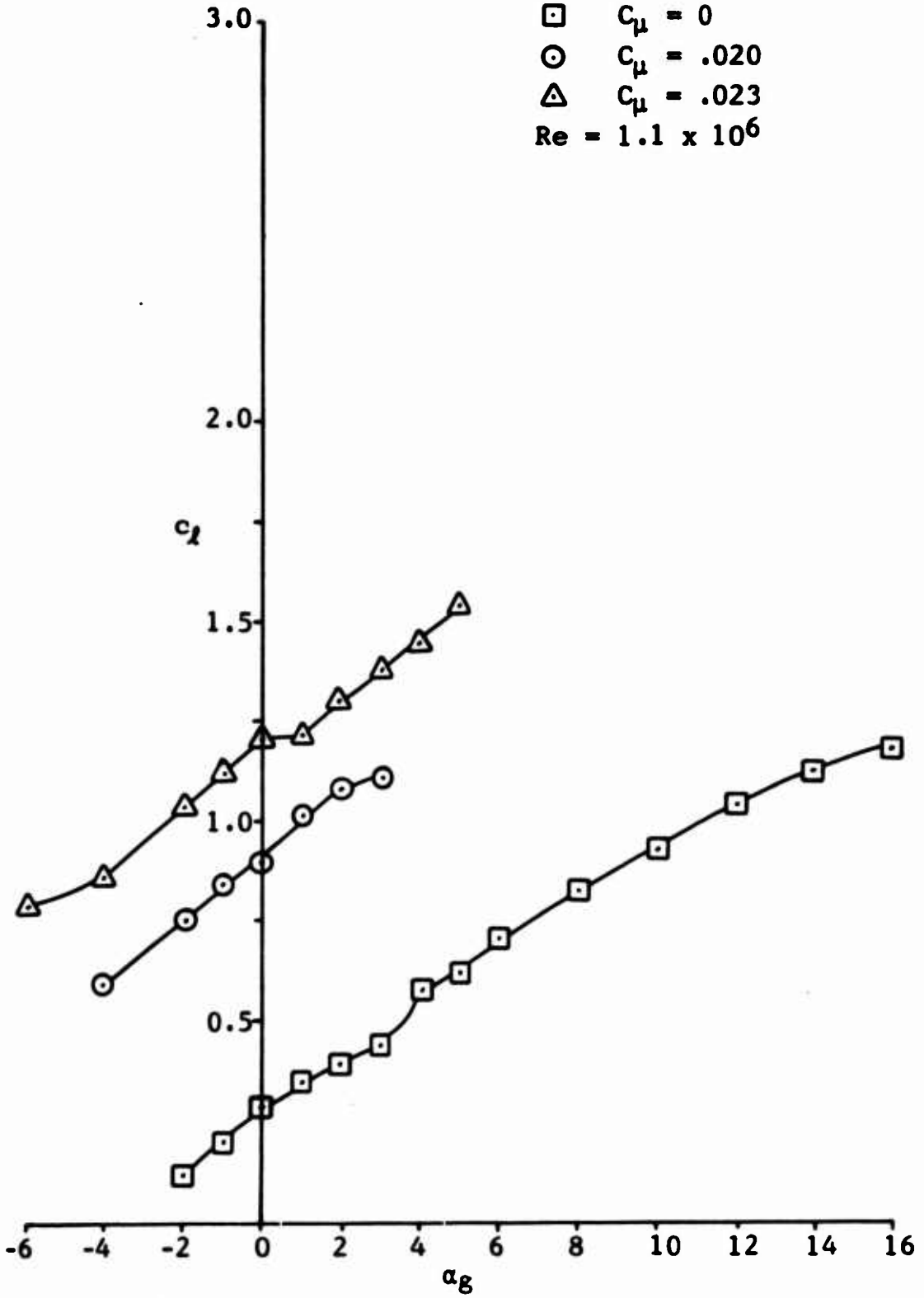

Figure 19. The Increase in c_ℓ vs α_g Due to Blowing at Various Momentum Coefficients on Model A, Without Splitter Plate

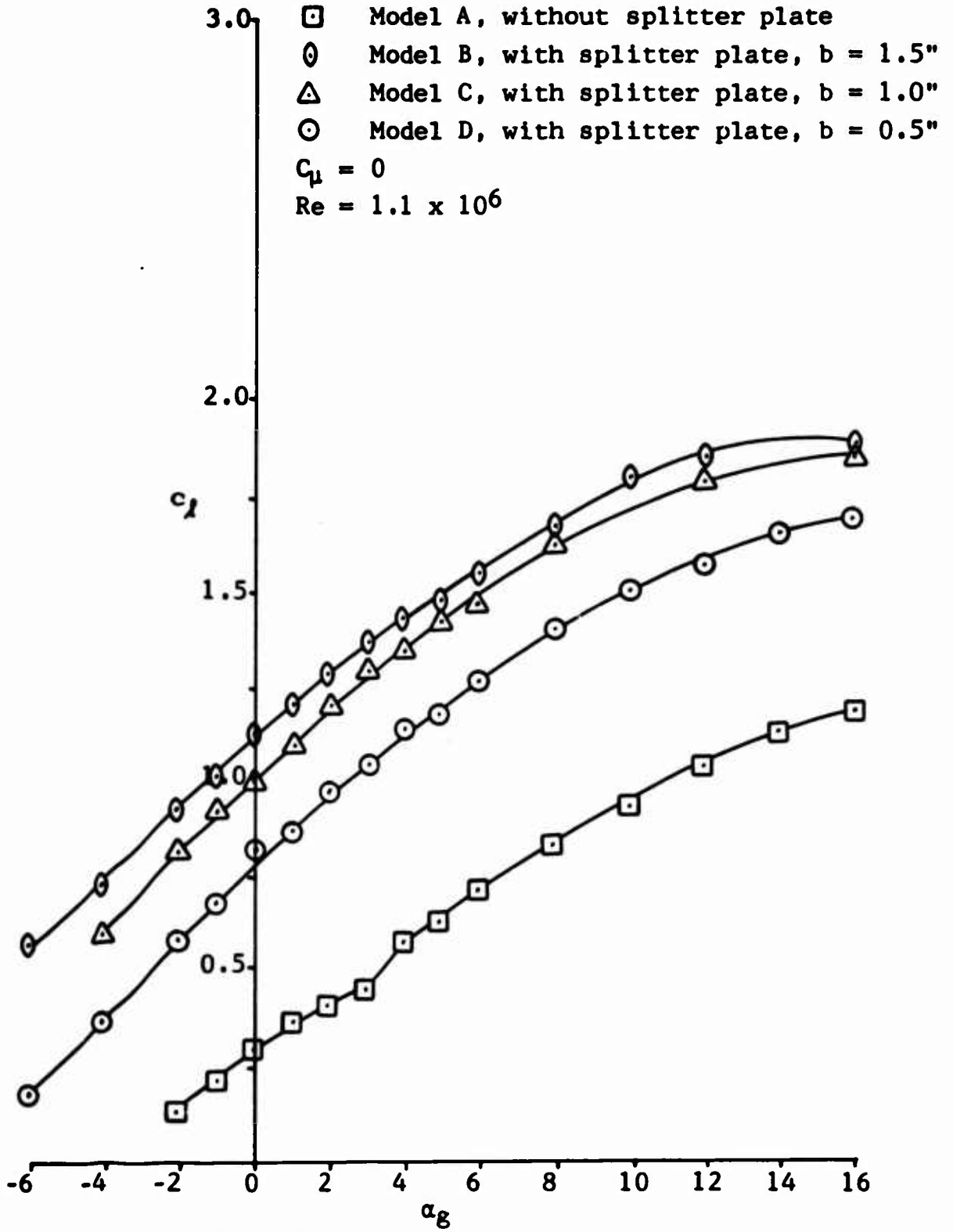

Figure 20. The Increase in c_ℓ vs α_g Due to the Splitter Plates

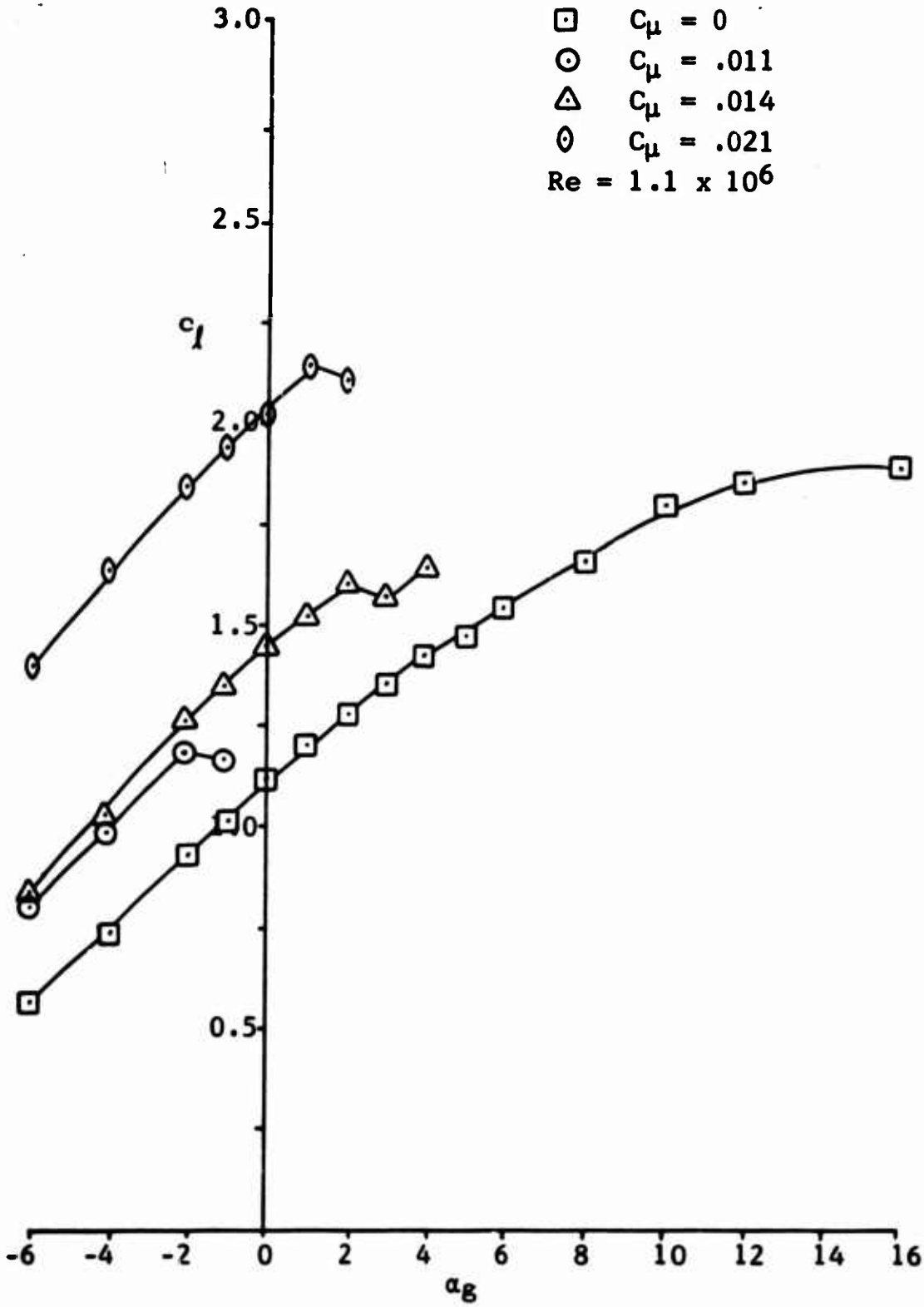

Figure 21. The Increase in c_ℓ vs α_g Due to Blowing at Various Momentum Coefficients on Model B, with Splitter Plate, b = 1.5 inches

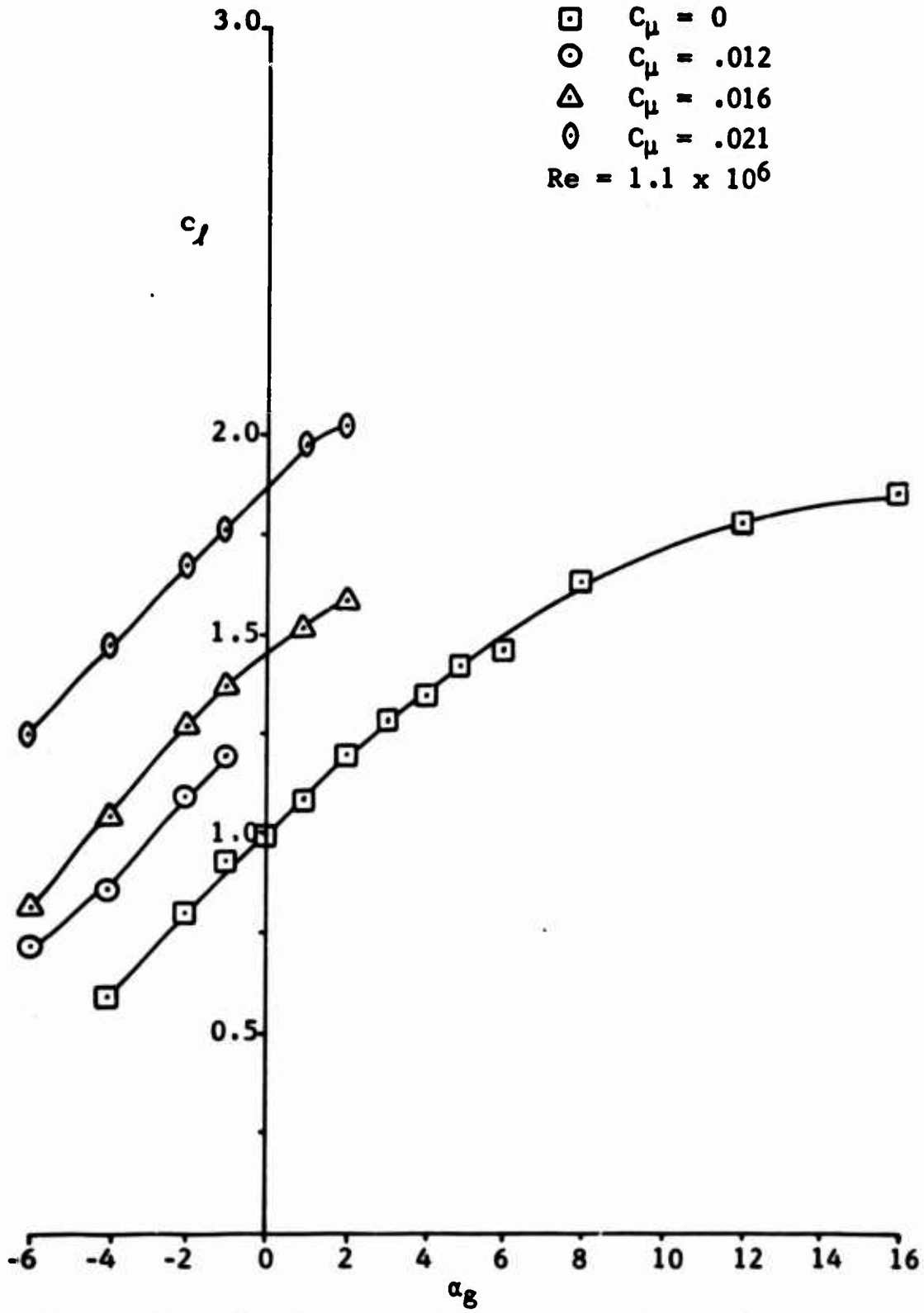

Figure 22. The Increase in c_ℓ vs α_g Due to Blowing at Various Momentum Coefficients on Model C, with Splitter Plate, b = 1.0 inches

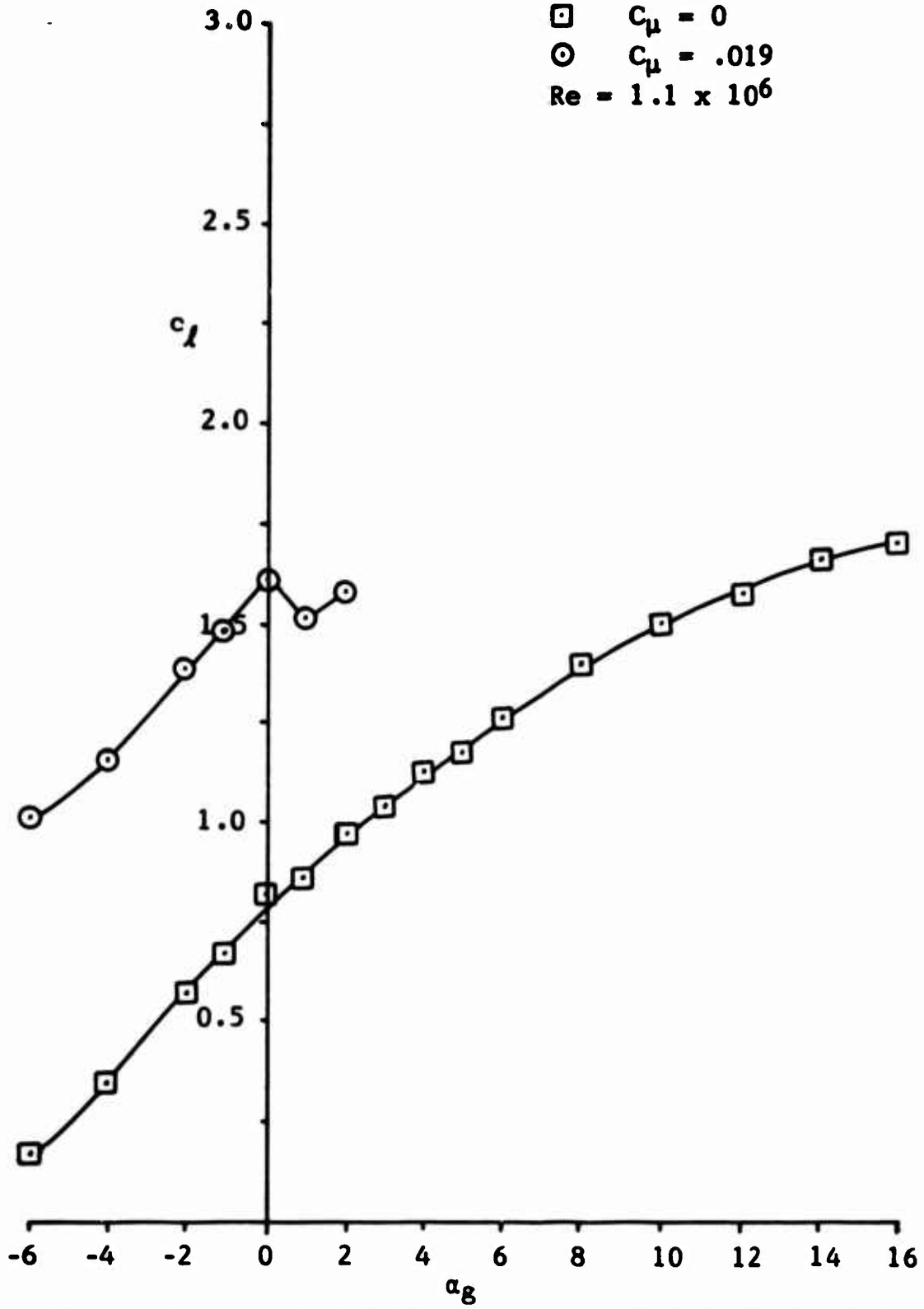

Figure 23. The Increase in c_ℓ vs α_g Due to Blowing on Model D, with Splitter Plate, b = 0.5 inches

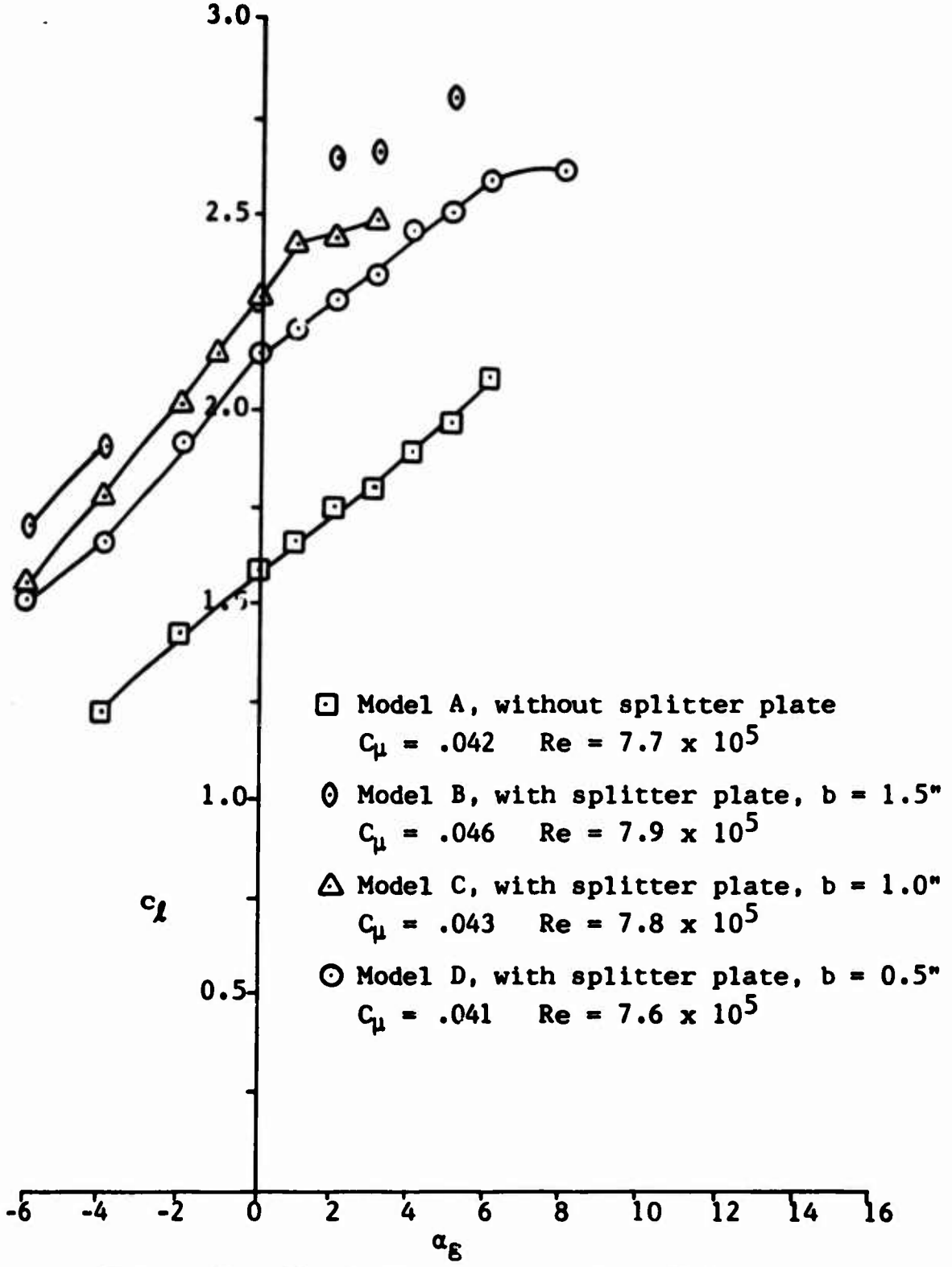

Figure 24. The Increase in c_ℓ vs α_g Due to the Splitter Plates with Blowing

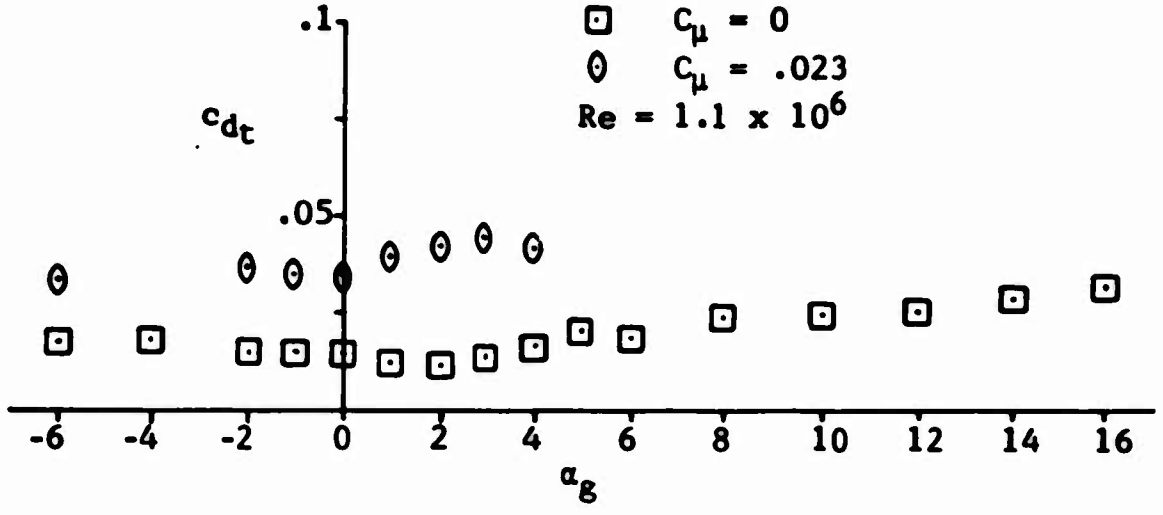

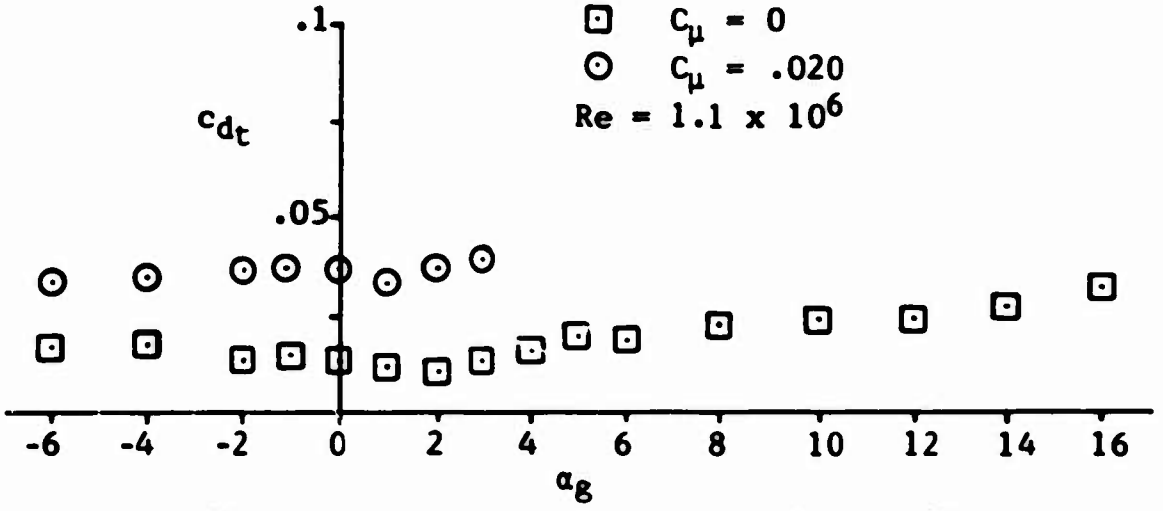

Figure 25. The Increase in c_{d_t} vs α_g Due to Blowing at Various Momentum Coefficients on Model A, Without Splitter Plate

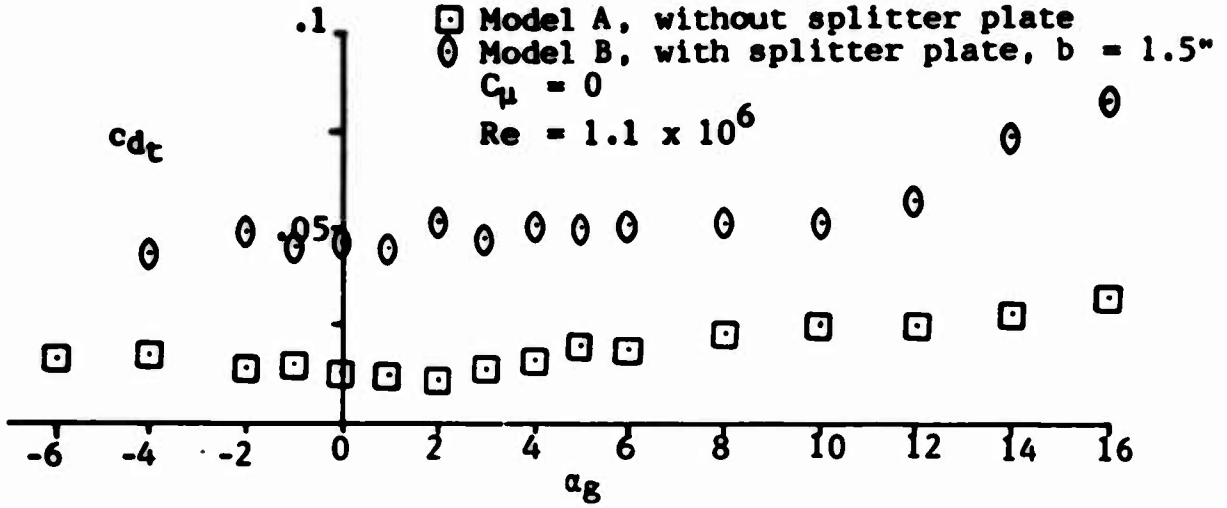

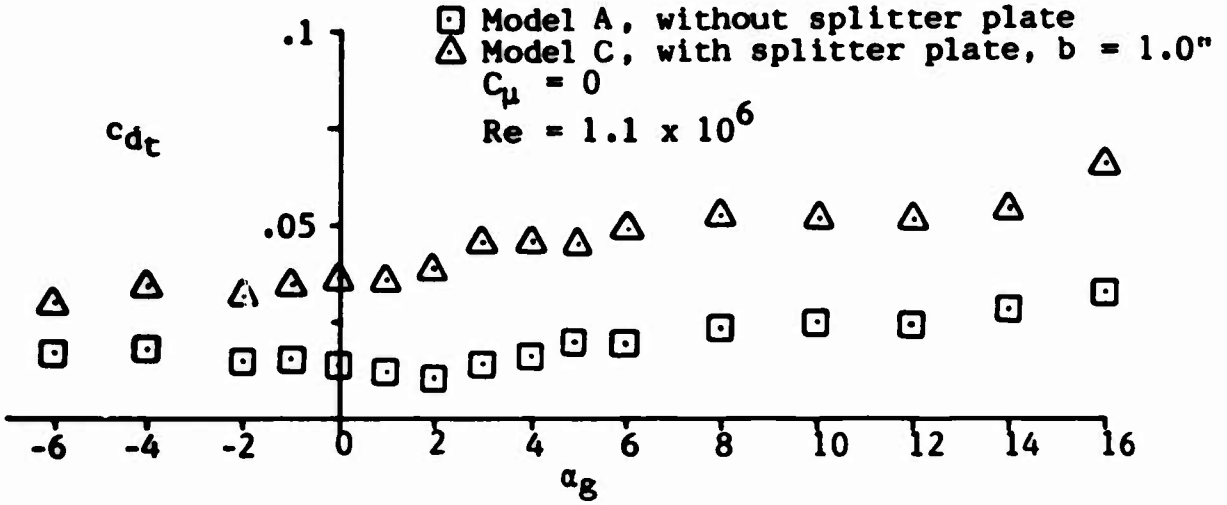

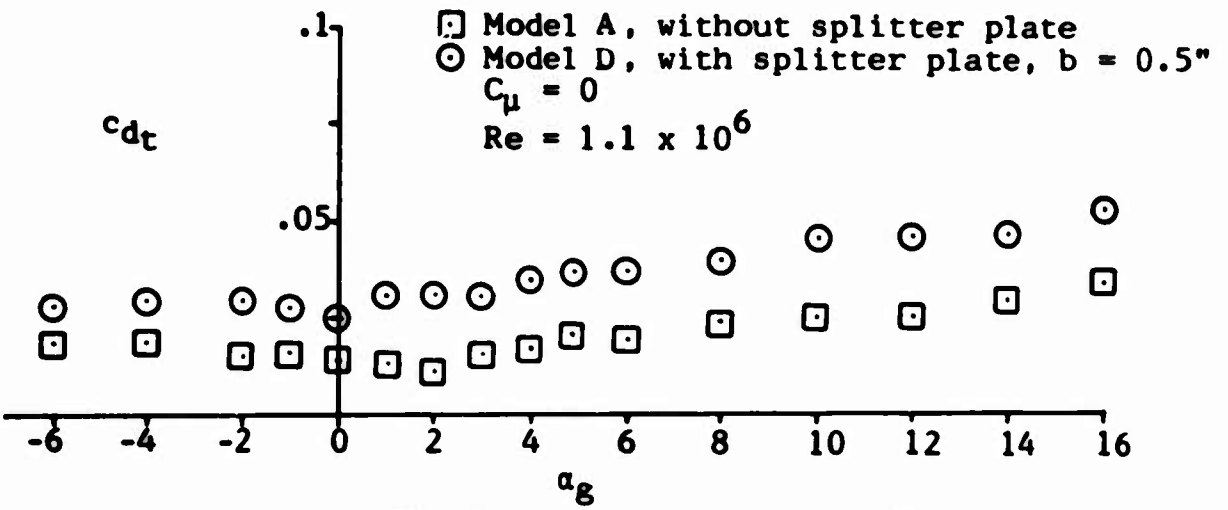

Figure 26. The Increase in c_{d_t} vs α_g Due to the Splitter Plates

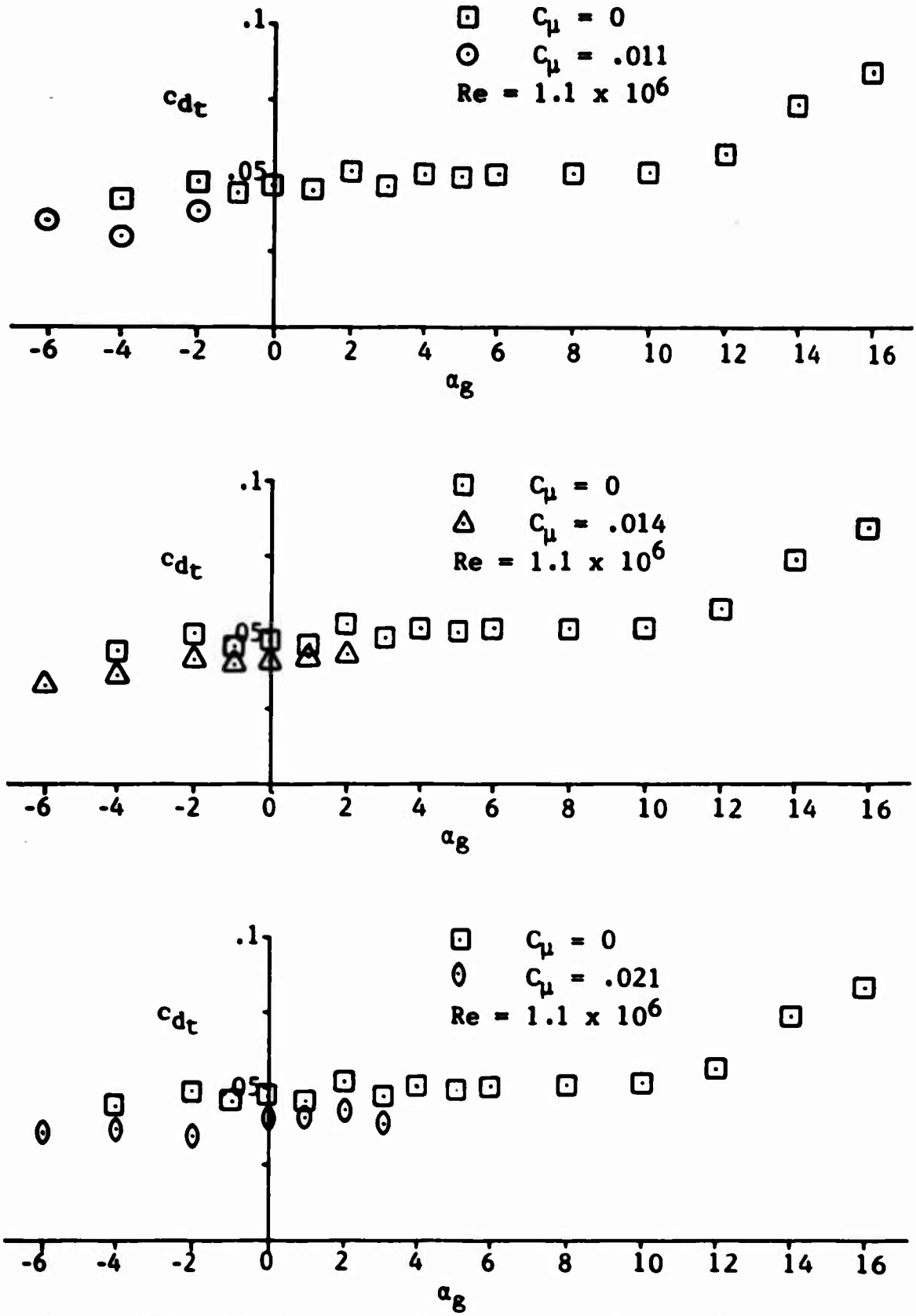

Figure 27. The Decrease in c_{d_t} vs α_g Due to Blowing at Various Momentum Coefficients on Model B, with Splitter Plate, b = 1.5 inches

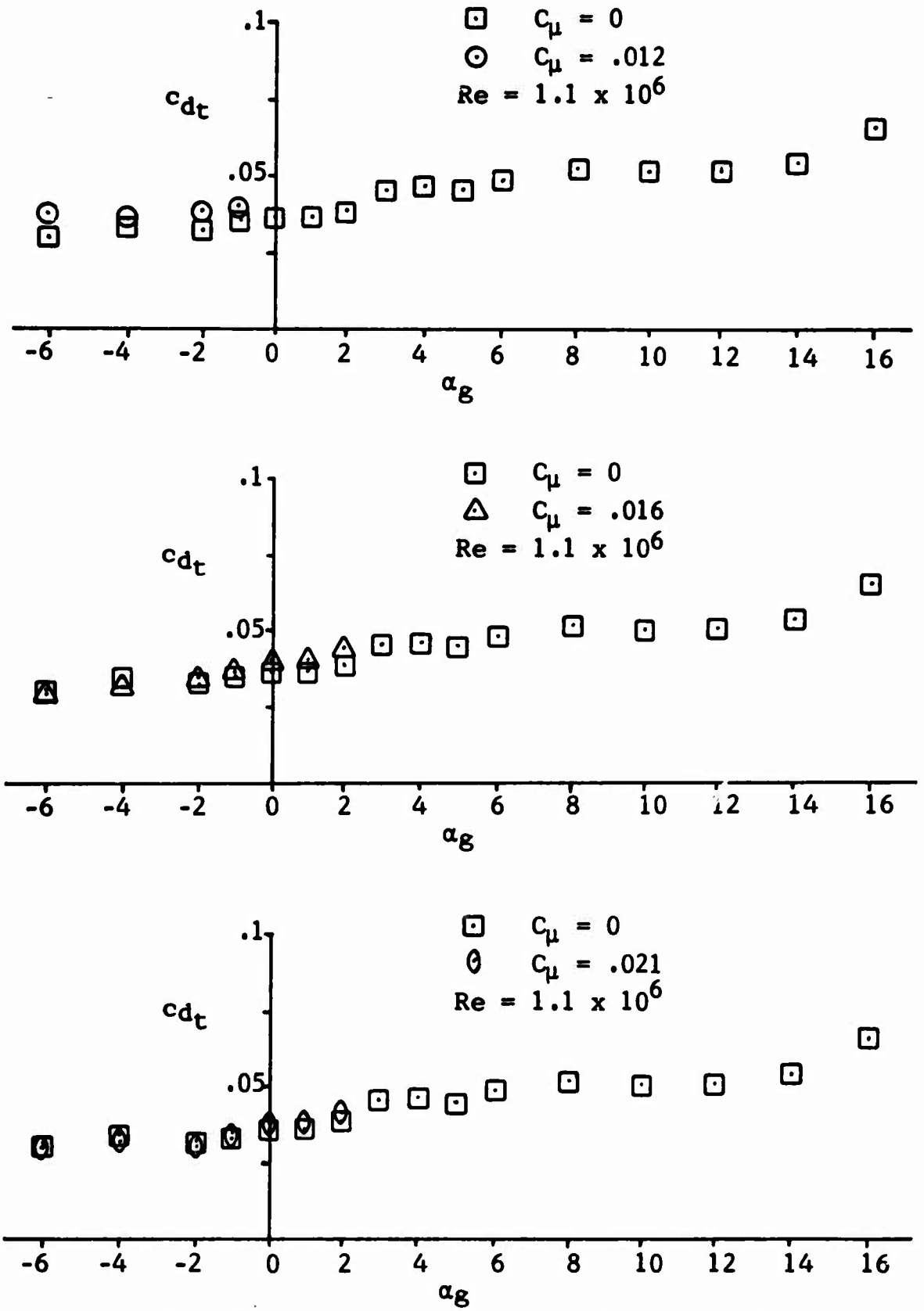

Figure 28. The Change in c_{d_t} vs α_g Due to Blowing at Various Momentum Coefficients on Model C, with Splitter Plate, b = 1.0 inch

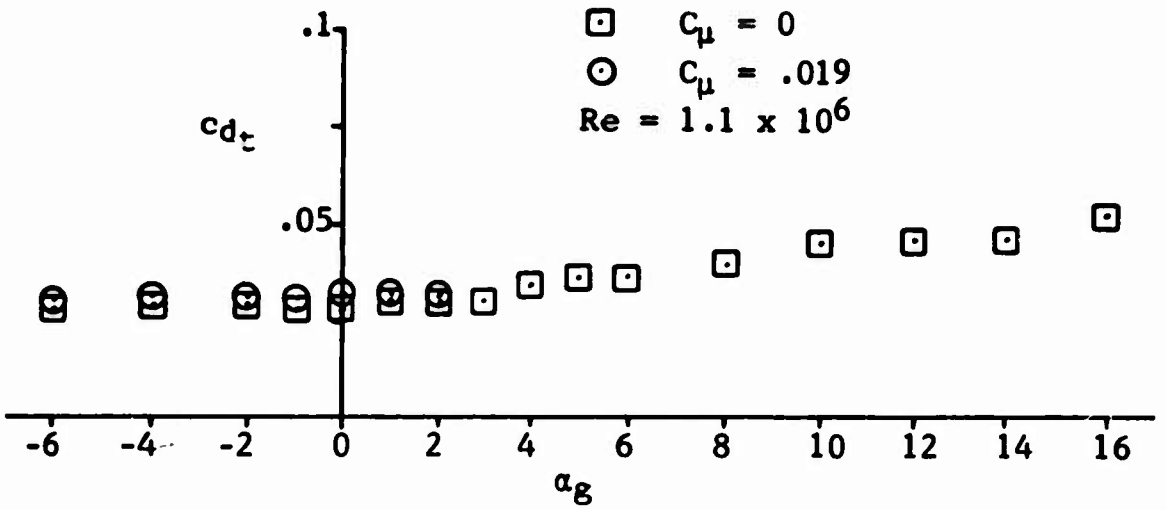

Figure 29. The Change in c_{d_t} vs α_g Due to Blowing on Model D, with Splitter Plate, b = 0.5 inches

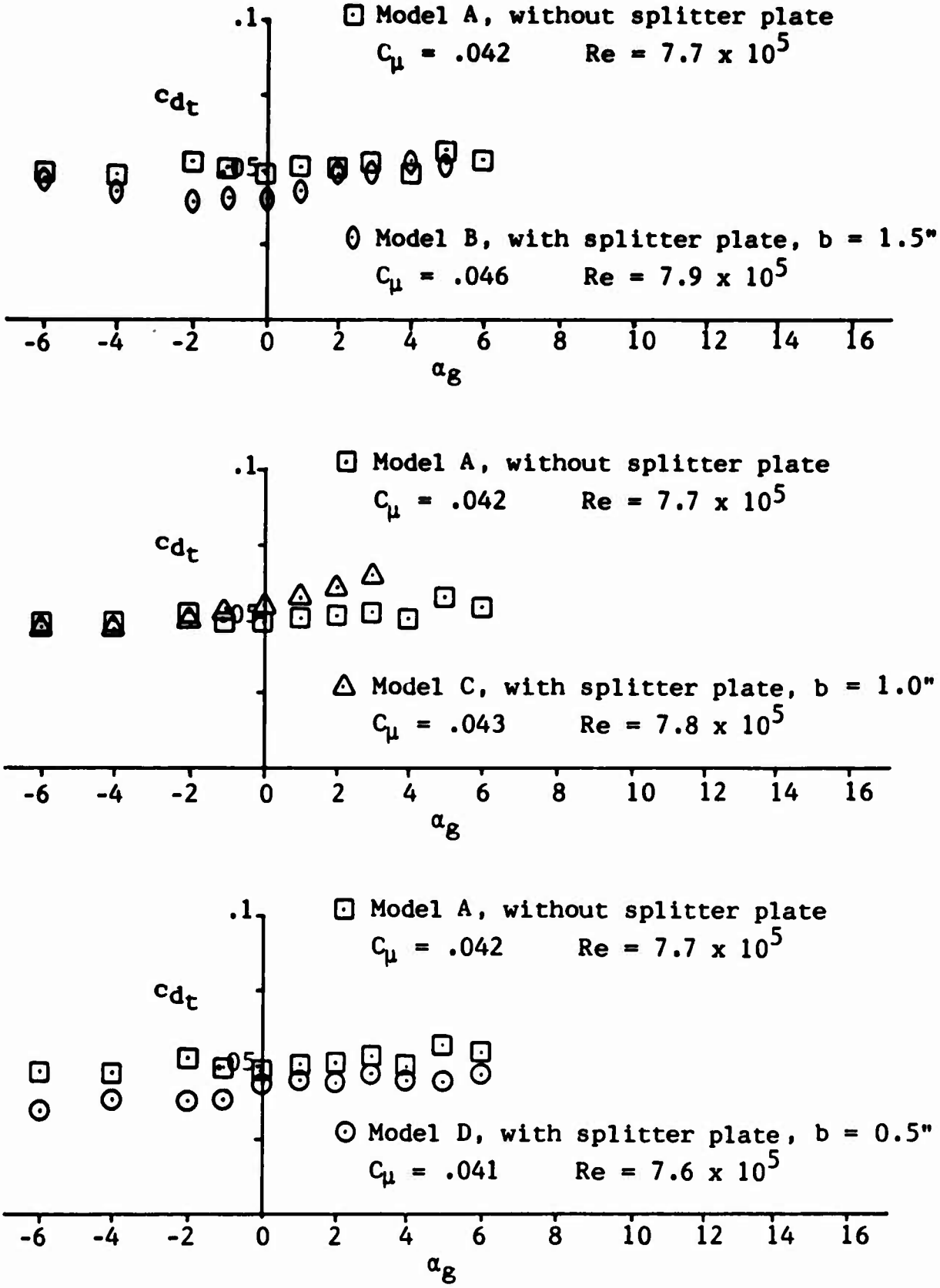

Figure 30. The Change in c_{d_t} vs α_g Due to the Splitter Plates with Blowing

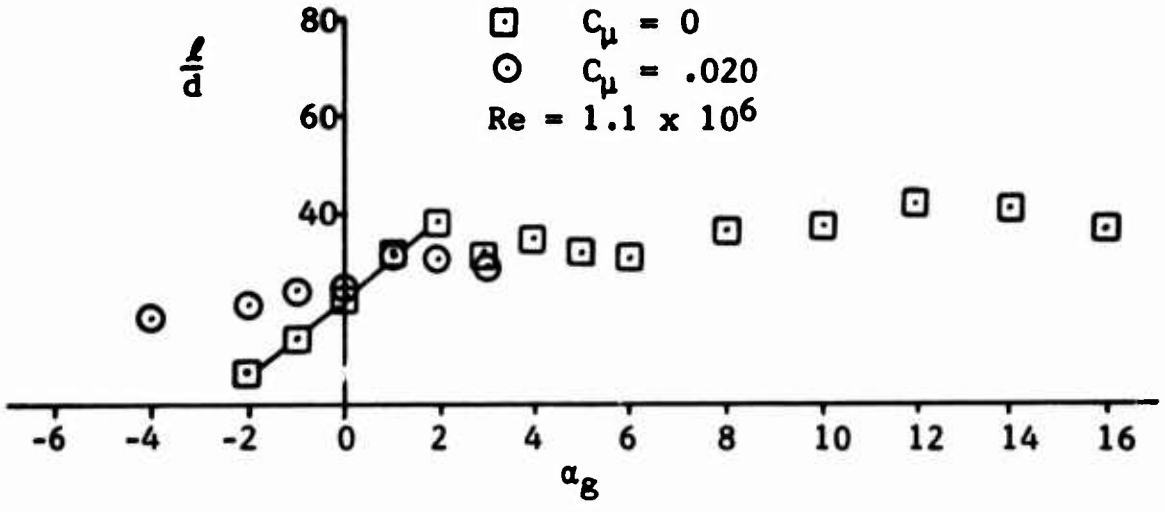

Figure 31. The Change in the Lift-to-Drag Ratio Due to Blowing on Model A, without Splitter Plate

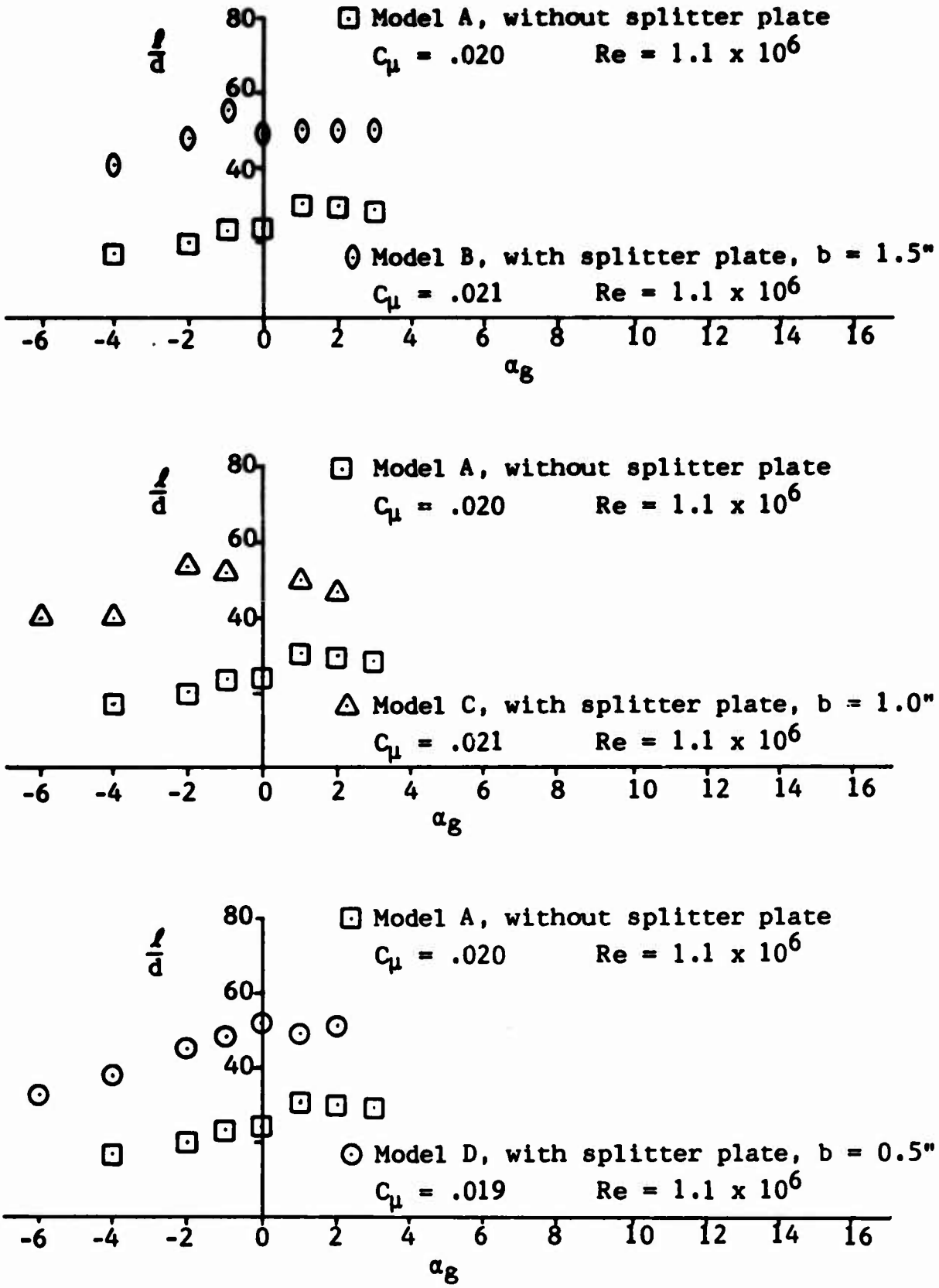

Figure 32. The Increase in the Lift-to-Drag Ratio Due to the Splitter Plates with Blowing

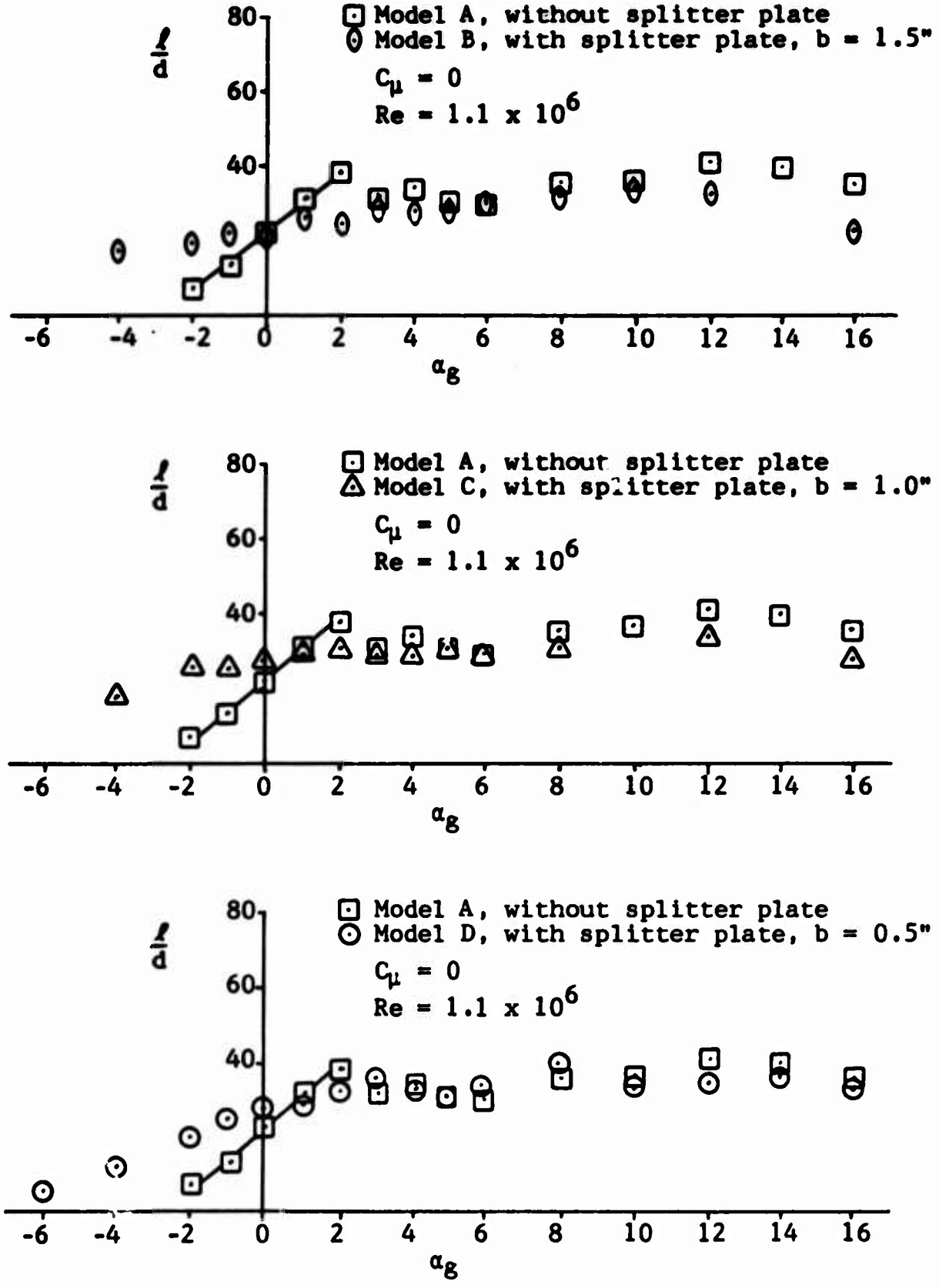

Figure 33. The Change in the Lift-to-Drag Ratio Due to the Splitter Plates

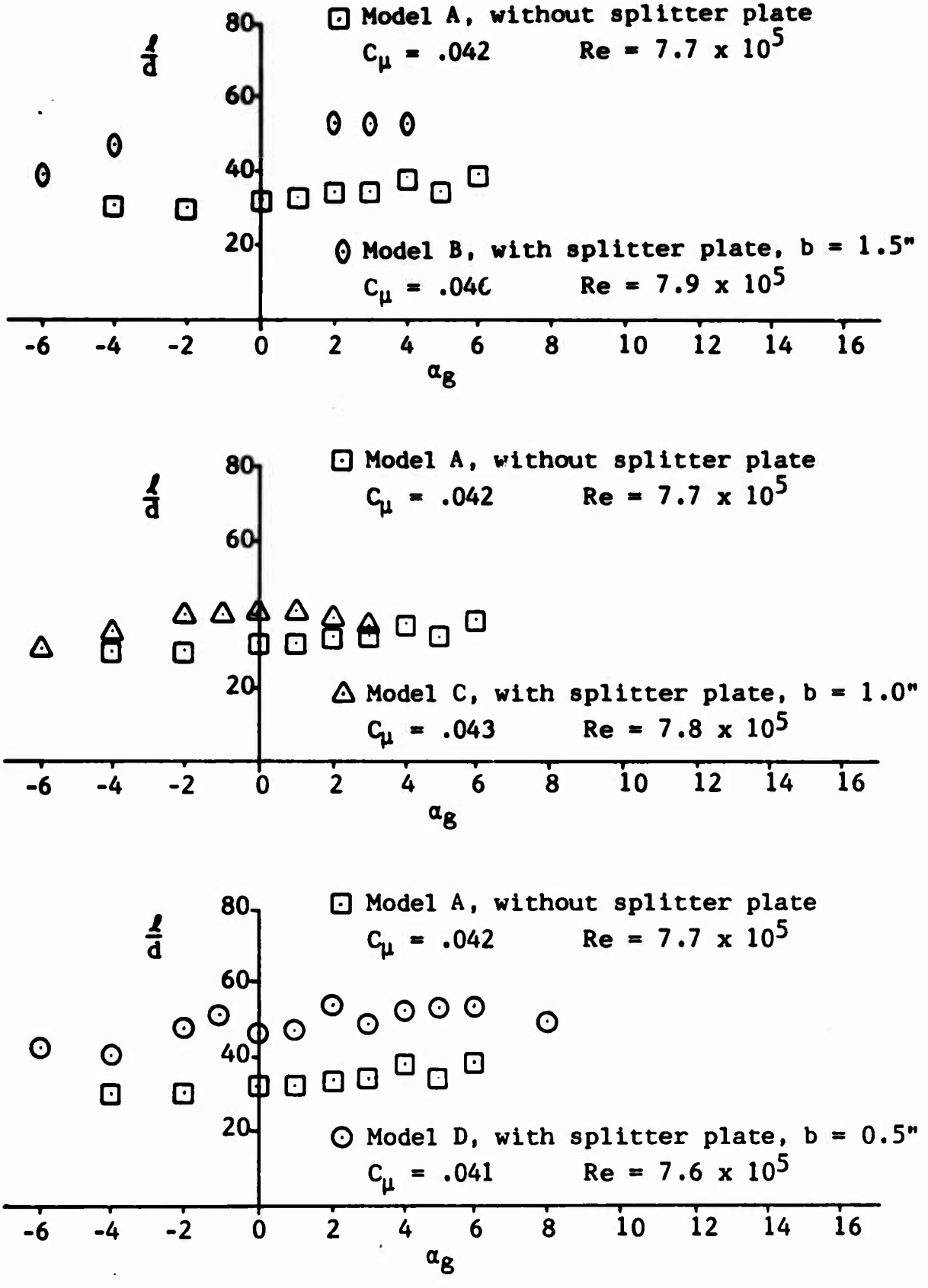

Figure 34. The Increase in the Lift-to-Drag Ratio Due to the Splitter Plates with Blowing

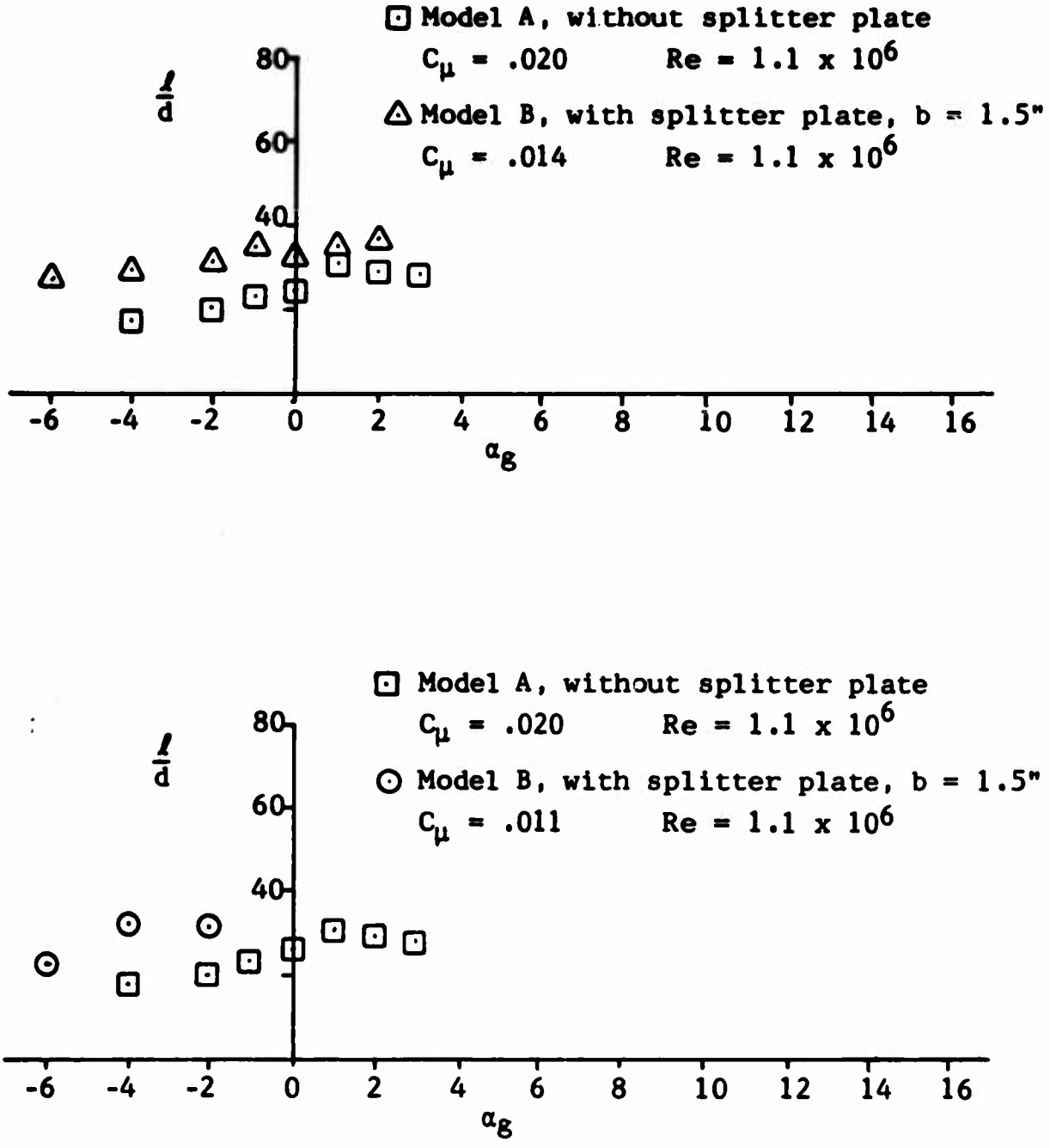

Figure 35. The Increase in the Lift-to-Drag Ratio Due to the Splitter Plate at Various Momentum Coefficients

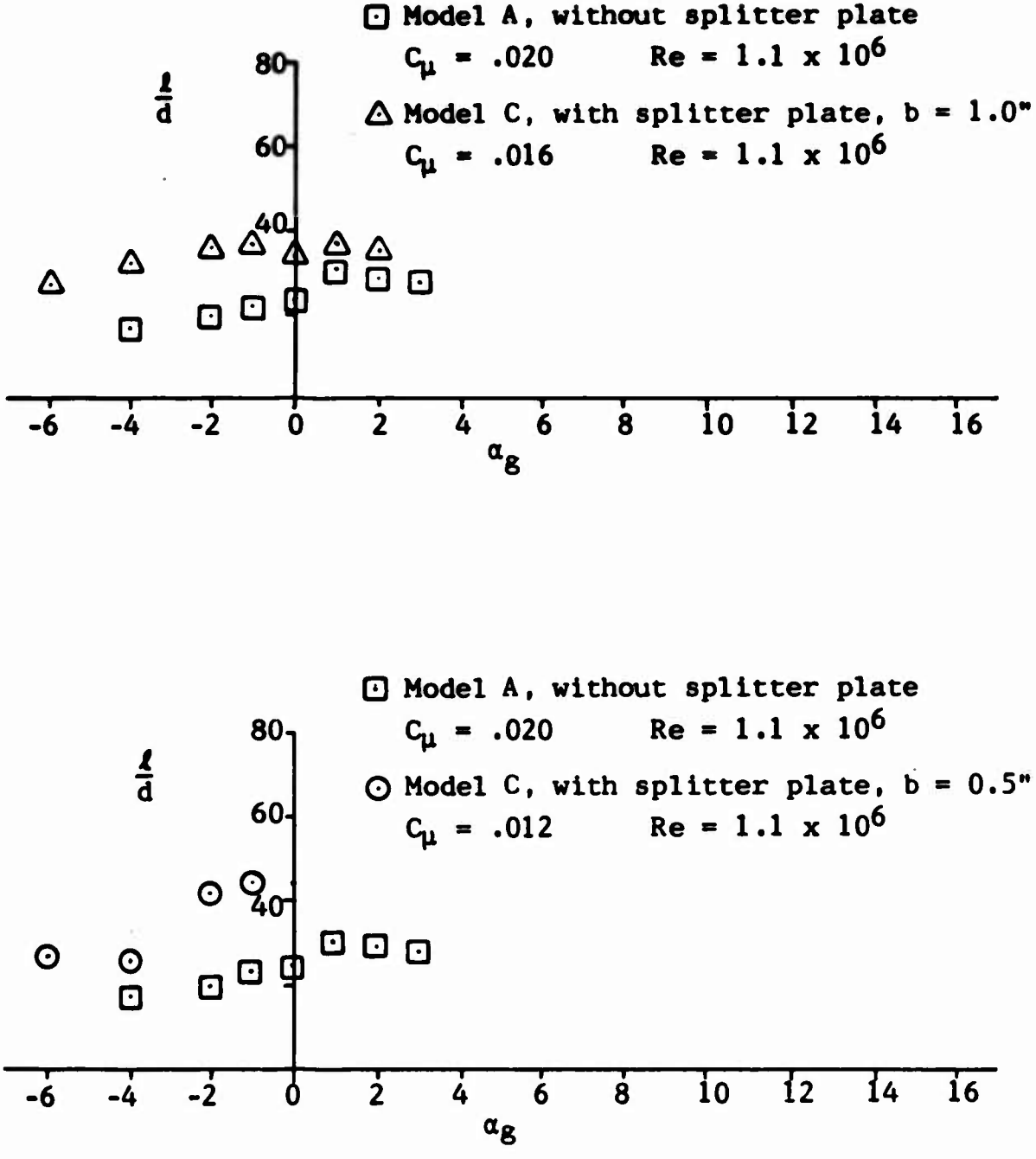

Figure 36. The Increase in the Lift-to-Drag Ratio Due to the Splitter Plate at Various Momentum Coefficients

Appendix B

The Procedure to Determine the Section Normal Force Coefficient

The static pressure of the airfoil center span was photographed during each wind tunnel test. After the test was complete the 35 mm film was developed. A 35 mm microfilm reader and printer was used to make eight by eleven inch prints of each of the sets of pressure data. Figure 37 shows a sketch of the static pressure distribution as it appeared on the microfilm print for one wind tunnel test. Each of the manometer readings in the figure represents the local static pressure at each pressure tap on the upper and lower surfaces of the model.

The Hewlett and Packard 9100A Calculator with 9107A Digitizer was used to compute the pressure coefficient at each pressure tap on the airfoil. The pressure coefficient is defined as:

$$C_p = \frac{P_\ell - P_o}{q_o} \qquad (3)$$

P_ℓ was read directly from the microfilm print. The calculator output the experimental pressure coefficient for each pressure tap on the airfoil. Thus, the experimental pressure coefficient could be compared to the potential flow theory pressure coefficient predicted for the test conditions. The section normal force coefficient was determined by a numerical integration of the pressure coefficients around

the airfoil. The integration was performed on the calculator using the trapezoidal rule of integration according to the equation:

$$c_n = \int_0^1 (C_{p_\ell} - C_{p_u}) \; d(\frac{x}{c}) \qquad (4)$$

The advantage of using the photographs to record the pressure was that the procedure was not as tedious as reading each pressure tube on the manometer bank during tests. Also all of the pressure tubes on the manometer bank were recorded simultaneously.

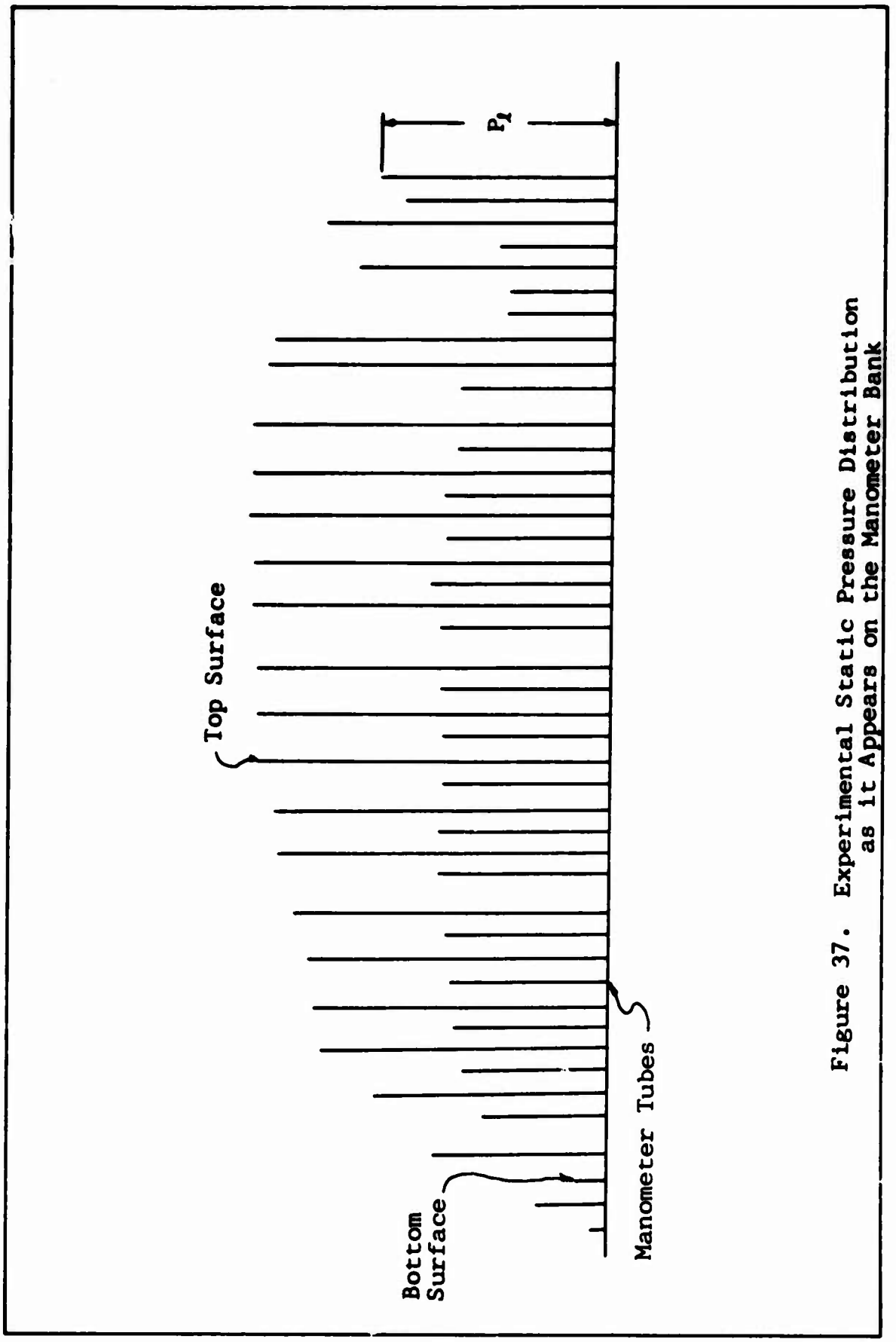

Figure 37. Experimental Static Pressure Distribution as it Appears on the Manometer Bank

Appendix C

The Procedure to Determine the Section Profile Drag Coefficient

The static and total pressure data obtained from the wake survey rake were photographed during each wind tunnel test. After the test was complete the 70 mm film was developed and nine by six inch prints were made from the negatives. Figure 38 shows the parameters of the wake profile which were contained on each of the negatives.

The parameters q and q_o were extracted directly from the photographs. The section profile drag coefficient was determined by a numerical integration over the tunnel cross section using the data from the photographs and the equation:

$$c_d = \frac{2}{c} \int_0^h \left[\sqrt{\frac{q}{q_o}} - \frac{q}{q_o} \right] dy \qquad (7)$$

The integration was performed using the trapezoidal rule of integration on the Hewlett and Packard 9100A Calculator with 9107A Digitizer.

The advantage of using the photographs was that the procedure was not as tedious as reading each pressure tube on the manometer bank during tests. Also all of the pressure tubes on the manometer bank were recorded simultaneously.

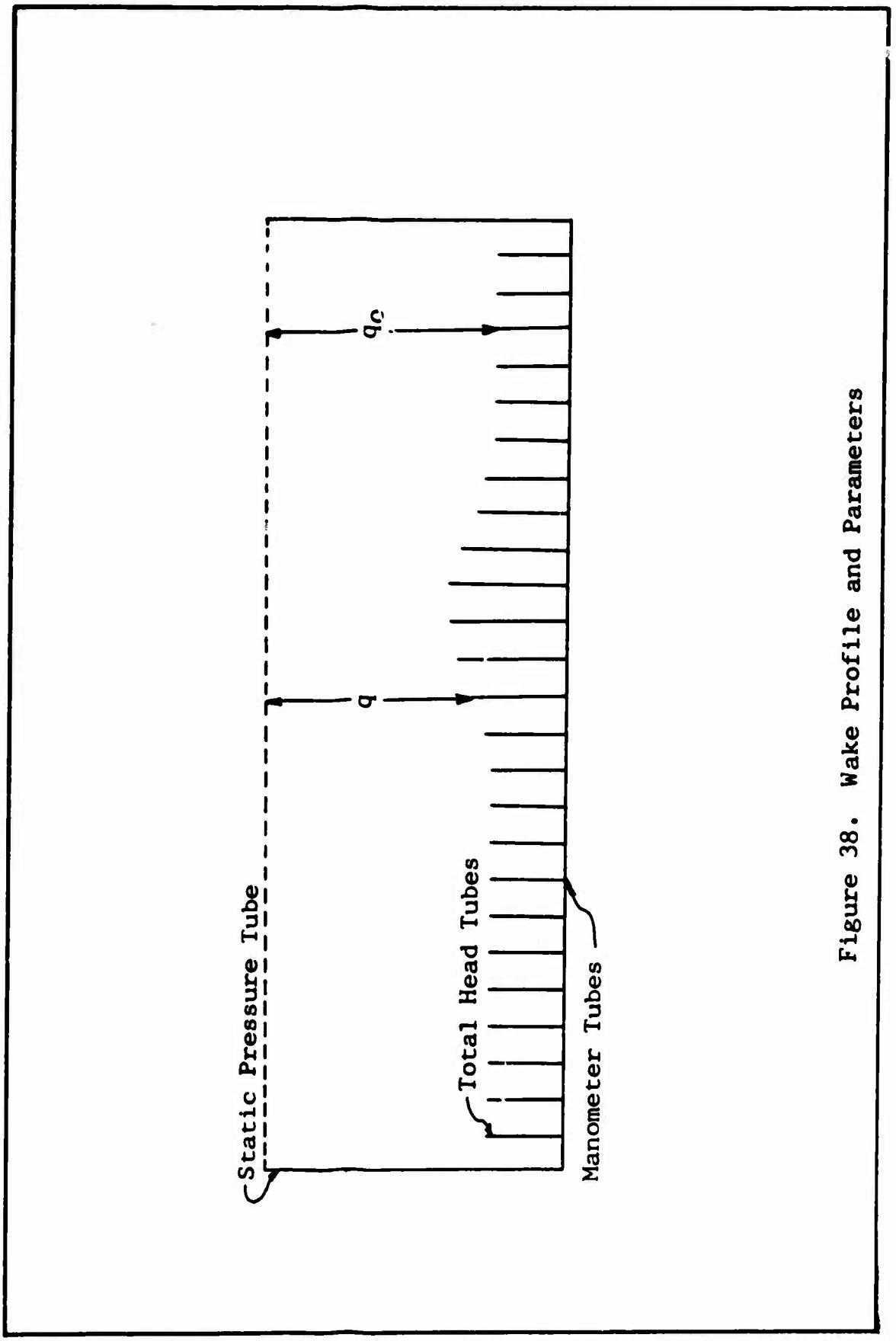

Figure 38. Wake Profile and Parameters

VITA

Thomas Adlai Stevenson was born [redacted] He graduated from [redacted] in 1962. He attended Sacramento City College in 1963 and then entered the United States Naval Academy where he received a Bachelor of Science degree and a commission in the United States Air Force in June 1967. After graduating from pilot training, he served as a UC-123K pilot in the 12th Special Operations Squadron, Danang Air Base, Republic of South Vietnam, and as a KC-135 pilot in the 915th Air Refueling Squadron, Ramey Air Force Base, Puerto Rico, and in the 91st Air Refueling Squadron, McConnell Air Force Base, Kansas. He enrolled in the Air Force Institute of Technology in December 1972.

Permanent address: [redacted]

This thesis was typed by Mrs. Robyn R. Stevenson